Available online at www.sciencedirect.com
SCIENCE DIRECT®
Journal of Non-Crystalline Solids 352 (2006) 2681–2714
JOURNAL OF NON-CRYSTALLINE SOLIDS
www.elsevier.com/locate/jnoncrysol

Review

Homogeneous crystal nucleation in silicate glasses: A 40 years perspective

Vladimir M. Fokin [a,*], Edgar D. Zanotto [b], Nikolay S. Yuritsyn [c], Jürn W.P. Schmelzer [d]

[a] *Vavilov State Optical Institute, ul. Babushkina 36-1, 193171 St. Petersburg, Russia*
[b] *LaMaV – Vitreous Materials Laboratory, Federal University of São Carlos, 13565-905 São Carlos, SP, Brazil*
[c] *Grebenshchikov Institute of Silicate Chemistry, Russian Academy of Sciences, ul. Odoevskogo 24-2, 199155 St. Petersburg, Russia*
[d] *Institut für Physik, Universität Rostock, 18051 Rostock, Germany*

Received 18 June 2005; received in revised form 27 January 2006
Available online 24 May 2006

Dedicated to the memory of Peter F. James

Abstract

We review a plethora of relevant experimental results on internal homogeneous crystal nucleation in silicate glasses obtained in the last four decades, and their analyses in the framework of the classical nucleation theory (CNT). The basic assumptions and equations of CNT are outlined. Particular attention is devoted to the analysis of the properties of the critical nuclei, which, to a large extent, govern nucleation kinetics. The main methods employed to measure nucleation rates are described and the possible errors in the determination of the crystal number density (and, correspondingly, in nucleation rates) are discussed. The basic regularities of both time and temperature dependencies of nucleation rates are illustrated by numerous experimental data. Experimental evidence for a correlation between maximum nucleation rates and reduced glass transition temperatures is presented and theoretically justified. Special attention is given to serious problems that arise in the quantitative description of nucleation rates when using the CNT, for instance: the dramatic discrepancy between calculated and measured nucleation rates; the high value of the crystal nuclei/melt surface energy, σ_{cm}, if compared to the expected value estimated via Stefan's rule; the increase of σ_{cm} with increasing temperature; and the discrepancies between the values of the surface energy and the time-lag for nucleation when independently estimated from nucleation and growth kinetics. The analysis of the above mentioned problems leads to the following conclusion: in contrast to Gibbs' description of heterogeneous systems underlying CNT, the bulk thermodynamic properties of the critical nuclei generally differ from those of the corresponding macro-phase resulting simultaneously in significant differences of the surface properties as compared with the respective parameters of the planar interfaces. In particular, direct experimental evidence is presented for compositional changes of the crystal nuclei during formation of the critical nuclei and their growth from critical to macro-sizes. In addition, detailed examinations of crystal nucleation and growth kinetics show a decrease of both the thermodynamic driving force for nucleation and of the critical nuclei/liquid interfacial energy, as compared with the respective properties of the macro-phase. However, despite significant progress in understanding crystal nucleation in glasses in the past four decades, many problems still exist and this is likely to remain a highly interesting subject for both fundamental and applied research for a long time.

Keywords: Crystallization; Glass ceramics; Nucleation; Crystals; Glass transition; Oxide glasses; Silicates; Thermodynamics

1. Introduction

Glasses can be defined as non-crystalline solids that undergo a *glass transition* in the course of their preparation. One of the most important and traditional (but not the only)

* Corresponding author. Address: ul. Nalichnay 21, ap.7, 199406 St. Petersburg, Russia. Tel.: +7 812 355 30 38.
E-mail address: vfokin@pisem.net (V.M. Fokin).

0022-3093/$ - see front matter © 2006 Elsevier B.V. All rights reserved.
doi:10.1016/j.jnoncrysol.2006.02.074

method of vitrification consists in supercooling a liquid escaping crystallization. Thus, when a liquid is cooled down at sufficiently high rates, crystallization can occur to a limited degree or can be completely arrested down to temperatures corresponding to very high viscosities, in the range $\eta \geqslant 10^{13}$–10^{12} Pa s $\approx \eta(T_g)$, where T_g is the glass transition temperature. Below this temperature, the viscosity is so high that large-scale atomic rearrangements of the system are no longer possible within the time-scale of typical experiments, and the structure freezes-in, i.e., the structural rearrangements required to keep the liquid in the appropriate metastable equilibrium state cannot follow any more the change of temperature. This process of freezing-in the structure of an undercooled liquid transforming it into a glass is commonly denoted as *glass transition*. Typical glass-forming liquids, such as silicate melts, are usually characterized by: (i) relatively high viscosities ($\eta > 100$ Pa s) at the melting point or liquidus and (ii) a steep increase of the viscosity with decreasing temperature. These properties favor vitrification. The mechanism above sketched leads to the conclusion that the glass structure must be similar to that of the parent undercooled liquid at temperatures near T_g and, indeed, this similarity has been experimentally observed.

Glass is thermodynamically unstable with respect to the undercooled liquid, i.e., there is no energy barrier between the glass and its corresponding undercooled (metastable) liquid. At a first glance, the high stability of the glassy state reflects only a relaxation problem; the system cannot evolve to a metastable state due to the kinetic inhibition of this process at low temperatures. On heating, relaxation of the glass structure may occur to reach first a metastable liquid state corresponding to the given temperature and then, eventually, go over into the crystalline state. The latter evolution process, as will be shown below, involves overcoming of a thermodynamic potential barrier. At room temperature glasses can exist for extremely long periods of time because their high viscosity inhibits structural rearrangements required for crystal nucleation and growth. However, when a glass is heat-treated for a sufficiently long time at temperatures within or above the glass transition range, devitrification readily starts, as a rule, from the surface and sometimes in the bulk via heterogeneous or homogeneous nucleation (see below).

Nucleation, or the process of formation of the precursors of the crystalline phases, may occur by different mechanisms. Commonly one divides these processes into homogeneous and heterogeneous nucleation. Homogeneous nucleation is a stochastic process occurring with the same probability in any given volume (or surface) element. Alternatively, nucleation occurring on preferred nucleation sites, e.g., such as pre-existing interfaces, previously nucleated phases, and surface defects, is denoted as heterogeneous nucleation. Depending on the location where nucleation takes places, volume (bulk) and surface crystallization can be distinguished.

Glass-forming melts are interesting models for studies of nucleation, growth and overall crystallization phenomena. Their high viscosities result in relatively low (measurable) rates of crystallization, which may permit detailed studies of nucleation and growth kinetics. *Homogeneous* nucleation can sometimes be observed at deep undercoolings ($T/T_m < 0.6$) because glass-forming melts are excellent solvents for solid impurities that thus only exist as ionic species when the liquid is vitrified. In addition, the rapid increase of viscosity with decreasing temperature makes it possible to 'freeze-in' different states of the crystallization process by quenching previously heat-treated specimens to room temperature. Hence, as it was figuratively said in Ref. [1], 'glasses did and may serve as the Drosophila of nucleation theory in order to test different approaches'. Moreover, silicate glass is one of the oldest materials produced by mankind, having its origin about 6000 years ago in ancient Mesopotamia [2], but are still gaining technological importance.

It is evident from the above discussion that crystallization and glass formation are competitive processes. In this way, in order to avoid uncontrolled crystallization of glassy articles one needs to know the main factors that govern crystal nucleation and growth. On the other hand, controlled nucleation and crystallization of glasses underlay the production of glass-ceramics invented in the mid-1950s [3], which are widely used in both domestic and high-technology applications. By the foregoing reasons, the investigation of glass crystallization kinetics is of great interest from both practical and theoretical points of view. Since, in many respects, the nucleation stage determines the pathways of overall crystallization, in this review we will focus our attention on nucleation, with particular emphasis on the analysis of relevant experimental results in the framework of the classical nucleation theory (CNT). Hereby we will restrict ourselves to selected data for homogeneous nucleation obtained mainly with silicate glasses.

The present paper is organized as follows: In Section 2, the basic equations of CNT are briefly summarized, which are then employed for nucleation data analysis. Section 3 presents the main methods that may by employed to experimentally determine nucleation rates. Section 4 is devoted to experimental findings concerning transient and steady-state crystal nucleation in glasses. In particular, evidence for a strong correlation between nucleation rates and reduced glass transition temperature is given. An analysis of the problems arising in the application of CNT to experimentally observed nucleation rate data is performed in Section 5. The paper is completed by concluding remarks.

2. Basic assumptions and equations of classical nucleation theory (CNT)

2.1. Historical notes

In its original form, classical nucleation theory is based on the thermodynamic description of heterogeneous systems developed by Gibbs [4]. Following Gibbs, a real inhomogeneous system is replaced by a model system consisting

of two homogeneous phases divided by a mathematical surface of zero thickness. While the properties of the ambient phase are known, the bulk properties of the critical clusters are determined via Gibbs' equilibrium conditions. A detailed analysis shows that the cluster bulk properties determined in such way are widely identical to the properties of the newly evolving macroscopic phase coexisting in stable equilibrium with the ambient phase at a planar interface. The free energy of the heterogeneous system – consisting of a cluster of the newly evolving phase in the ambient phase – is expressed as the sum of the bulk contributions of the nucleus and the ambient phase. These bulk terms are supplemented by interfacial contributions, the main one is given by the product of the interfacial area and specific surface energy.

When applying the theory to cluster formation, these surface terms initially result in an increase of the characteristic thermodynamic potential, which leads to the existence of a critical cluster size. Only clusters with sizes larger than the critical size are capable to grow up to macroscopic dimensions in a deterministic way. The change of the characteristic thermodynamic potential resulting from the formation of clusters of critical size is commonly denoted as the work of critical cluster formation. This quantity reflects the thermodynamic aspects in the description of nucleation.

In addition to thermodynamic aspects of nucleation, the dynamics of cluster formation and growth must be appropriately incorporated into the theory. Different approaches have been employed depending on the particular problem being analyzed. The application of CNT to the formation of crystals originates from the work of Kaischew and Stranski [5]. These authors investigated this problem for the case of crystal formation from supersaturated vapor employing the approach developed by Volmer and Weber [6] for vapor condensation. Further advances in CNT including nucleation in the condensed systems, which are the focus of the present review, were connected with the work of Becker and Döring [7], Volmer [8], Frenkel [9], Turnbull and Fisher [10], Reiss [11] and others. Photographs of some of these pioneers of nucleation theory are shown in Fig. 1.

According to CNT, the description of homogeneous and heterogeneous nucleation can be basically performed by the same methods. We will present first the results for homogeneous nucleation and afterwards will introduce the modifications required to account for the effect of insoluble solid impurities and interfaces that may lead to heterogeneous nucleation.

2.2. Homogeneous nucleation

As we already discussed, homogeneous nucleation supposes the same probability of critical nucleus formation in any given volume or surface element of the system under

Fig. 1. From top left to right bottom: J.W. Gibbs, G. Tammann, M. Volmer, R. Kaischew, J. Frenkel, and D. Turnbull.

study. According to CNT (see, e.g., Refs. [12,13]), the steady-state homogeneous volume nucleation rate can be written as

$$I_{st} = I_o \exp\left[-\frac{W_* + \Delta G_D}{k_B T}\right], \qquad I_o = 2N_1 \frac{k_B T}{h}\left(\frac{a^2 \sigma_{cm}}{k_B T}\right)^{1/2}. \tag{1}$$

This equation determines the so-called steady-state nucleation rate, I_{st}, i.e., the number of supercritical clusters formed per unit time in a unit volume of the system. The pre-exponential term, I_o, depends only weakly on temperature (if compared to the exponential function) and varies between 10^{41} and 10^{43} m^{-3} s^{-1} for different condensed systems [14]. In Eq. (1) k_B and h are the Boltzmann and Planck constants, respectively; $N_1 \sim 1/a^3$ is the number of structural (formula) units, with a mean size a, per unit volume of melt; σ_{cm} is specific surface free energy of the critical nucleus-melt interface; ΔG_D is the activation free energy for transfer of a 'structural unit' from the melt to a nucleus (kinetic barrier). To a first approximation, the kinetic barrier for glass-forming liquids is often replaced by the activation free energy for viscous flow, ΔG_η. W_* is the thermodynamic barrier for nucleation, i.e., the increase in the free energy of a system due to the formation of a nucleus with critical size, r_*. The critical nucleus size can be determined from the condition

$$\frac{\partial W}{\partial r} = 0, \quad W = c_1 r^2 \sigma_{cm} - c_2 r^3 \Delta G_V, \tag{2}$$

where $\Delta G_V = G_l - G_c$ is the difference between the free energies of liquid and crystal per unit volume of the crystal (i.e., the thermodynamic driving force for crystallization) and c_1 and c_2 are shape factors. In the case of a spherical nucleus, we obtain the expressions

$$r_* = \frac{2\sigma_{cm}}{\Delta G_V} \tag{3}$$

and

$$W_* = \frac{16\pi}{3}\frac{\sigma_{cm}^3}{\Delta G_V^2}. \tag{4}$$

The thermodynamic driving force for crystallization is given by

$$\Delta G_V V_m = \frac{\Delta H_m}{T_m}(T_m - T) - \int_T^{T_m} \Delta C_p \, dT' + T\int_T^{T_m} \frac{\Delta C_p}{T'} dT', \tag{5}$$

where V_m is the molar volume, ΔH_m and T_m are the molar heat of melting and the melting temperature of the crystal, respectively, and $\Delta C_p = C_p^l - C_p^c$ is the difference between the molar heat capacities of liquid and crystal at constant pressure. The experimental values of ΔG_V are normally bounded by the approximations usually assigned to Turnbull (Eq. (6)) and Hoffman (Eq. (7)) that assume $\Delta C_p = 0$ and $\Delta C_p =$ constant, respectively [13],

$$\Delta G_V(T) = \Delta H_V\left(1 - \frac{T}{T_m}\right), \tag{6}$$

$$\Delta G_V(T) = \Delta H_V\left(1 - \frac{T}{T_m}\right)\frac{T}{T_m}. \tag{7}$$

Here ΔH_V is the melting enthalpy per unit volume of the crystal. One should note, however, that Eq. (6) was first employed by Thomson and Volmer (cf. Ref. [8]).

Eq. (1) describes the time-independent steady-state nucleation. Such nucleation regime occurs if a stationary size distribution of the newly evolving subcritical ($r < r_*$) and critical ($r = r_*$) nuclei is established in the system. The cooling rates typically employed for glass formation from the melt, and the heating rates of small glass specimens to any given temperature T under investigation are commonly too high to maintain a steady-state distribution of nuclei in the system. Hence, some time period is needed for a reconstruction of the initial nuclei distribution towards the time-independent distribution corresponding to the temperature of study. During this period the nucleation rate varies and approaches a steady-state value given by Eq. (1).

The time required to establish steady-state nucleation in a system is commonly denoted as the time-lag for nucleation, τ. It characterizes the duration for the onset of the steady-state distribution, and hence the evolution of the nucleation rate, $I(t)$, towards a steady-state value, I_{st}. In the cases when the initial concentration of critical and sub-critical nuclei may be neglected, τ and $I(t)$ can be expressed by Eqs. (8) and (9), respectively [15,16],

$$\tau = \frac{16h}{\pi}\frac{\sigma_{cm}}{\Delta G_V^2 a^4}\exp\left(\frac{\Delta G_D}{k_B T}\right), \tag{8}$$

$$I(t) = I_{st}\left[1 + 2\sum_{m=1}^{\infty}(-1)^m \exp\left(-m^2\frac{t}{\tau}\right)\right]. \tag{9}$$

Integration of Eq. (9) results in the following expression for the time-dependence of the number of super-critical nuclei per unit volume of the system, N_V,

$$\frac{N_V(t)}{I_{st}\tau} = \left[\frac{t}{\tau} - \frac{\pi^2}{6} - 2\sum_{m=1}^{\infty}\frac{(-1)^m}{m^2}\exp\left(-m^2\frac{t}{\tau}\right)\right]. \tag{10}$$

For sufficiently long times, t, as compared with τ this expression can be approximated by

$$N_V(t) = I_{st}\left(t - \frac{\pi^2}{6}\tau\right). \tag{11}$$

For the experimental estimation of τ, it is convenient to use the induction period, t_{ind}, defined via Eq. (12) as

$$\tau = \frac{6}{\pi^2} t_{ind}. \tag{12}$$

The induction period, t_{ind}, is easily determined as the intersection of the asymptote (Eq. (11)) with the time-axis. Another more correct way to estimate I_{st} and τ is by fitting the experimental values of $N(t)$ to Eq. (10).

2.3. Heterogeneous nucleation

The existence of foreign solid particles and phase boundaries may favor nucleation. This effect is due mainly to the diminished thermodynamic barrier as compared to that for homogeneous nucleation, owing to a decrease of the contribution of the effective surface energy to the work of critical cluster formation. For example, the thermodynamic barrier for nucleation in the case of condensation on planar interfaces is given by [12]

$$W_*^{\text{het}} = W_* \Phi, \quad \Phi = \tfrac{1}{2} - \tfrac{3}{4}\cos\theta + \tfrac{1}{4}\cos^3\theta. \tag{13}$$

Depending on the value of the wetting angle, θ, the parameter Φ varies from zero to unity. The value of Φ depends on the mechanism of nucleation catalysis.

In order to adapt the expression for the steady-state nucleation rate, Eq. (1), to the description of heterogeneous nucleation, the number of 'structural' units per unit volume, N_1, which appears in the pre-exponential term of Eq. (1), must be replaced by the number, N^S, of 'structural units' in contact with the catalyzing surface per unit volume. Hence, in the case of heterogeneous nucleation, the following equation can be written for the steady-state nucleation rate:

$$I_{\text{st}}^{\text{het}} \cong N^S \frac{k_B T}{h} \exp\left[-\frac{W_* \Phi + \Delta G_D}{k_B T}\right]. \tag{14}$$

Catalyzing surfaces may be represented, for instance, by dispersed solid particles that act as nucleation sites. In this case, their curvature and number may strongly affect the nucleation kinetics [14,17]. The exhaustion of available nucleation sites due to crystal nucleation leads to saturation of the kinetic curve N versus t. If, however, for some reason such saturation is not achieved, the knowledge of the $N(t)$-dependence is not sufficient to conclude what type of nucleation took place.

3. Experimental methods to estimate nucleation rates

3.1. General problem

At high undercoolings corresponding to the range of measurable homogeneous (volume) nucleation rates in typical glass-forming liquids, the critical nuclei are undetectable by common experimental techniques, hence they must first be developed to a visible size to allow one to determine (e.g., using a microscope) their number density, N, as a function of time, allowing then to estimate the nucleation rate as $I = \mathrm{d}N/\mathrm{d}t$. In order to perform such task, different methods have been developed.

3.2. Double-stage ('development') method

If the overlapping of the nucleation and growth rate curves is weak (i.e., the crystal growth rates are very low at temperatures corresponding to high nucleation rates), the observation of the nucleated crystals and the estimation of the crystal number density is a quite difficult task. For these cases, about a hundred years ago, Gustav Tammann (who was studying crystallization of organic liquids) proposed the following procedure, which is now known as the Tammann or 'development' method [18]. Crystals nucleated at a low temperature, T_n, are grown up to microscopic sizes at a higher temperature, $T_d > T_n$. The development temperature T_d has to meet the following conditions for nucleation (I) and growth (U) rates: $I(T_d) \ll I(T_n)$ and $U(T_d) \gg U(T_n)$. After a lapse of seventy years, Ito et al. [19] and Filipovich and Kalinina [20] independently applied Tammann's method to the study of crystal nucleation kinetics in lithium disilicate glasses. Since then, this method has been widely employed for glass crystallization studies. Some problem inherent in this method and connected with the possible dissolution of some part of the originally formed (at the nucleation temperature) nuclei at the development temperature will be discussed later.

3.3. Single-stage methods

3.3.1. The direct method

When there is considerable overlap of the $I(T)$ and $U(T)$-curves, the number density of crystals can be measured directly after single-stage heat treatments at T_n. Then, the obtained $N(T_n, t)$-curve will be shifted (relatively to the true one) to higher times by a time $t_o = (r_{\text{res}} - r_*)/U(T_n) \cong r_{\text{res}}/U(T_n)$ that is needed to grow the crystals up to the microscope resolution limit, $\varepsilon = 2r_{\text{res}}$ [21]. Finally, one must correct the number densities to account for stereological errors. This procedure will be described in Section 3.4.

3.3.2. Crystal size distribution analysis

Continuous nucleation and growth normally result in a broad distribution of crystal sizes, i.e., the first nucleated crystal has the largest size and so forth. If the crystal growth rate is known, one can calculate the 'birth dates' of crystals belonging to different size groups and then plot a $N(t)$-curve. Toschev and Gutzow derived the basic formulas relating the size distribution of spherical isolated particles embedded in a continuous matrix with that of their circular intersections on a sample cross-section for both steady-state and transient volume nucleation [22]. For surface crystallization the size distribution is easily constructed from direct measurements. This method, known as Köster's method, also works in the case of heterogeneous nucleation from a finite number of active centers when the latter are depleted in a relative short time, and further advancement of crystallization only occurs via crystal growth. It has been systematically employed to study the surface nucleation rates in metallic [23] and silicate glasses [24].

3.4. Stereological corrections

The use of reflected light microscopy can lead to large errors in the determination of the number of crystals per

unit volume due to the stereological methods employed to calculate volume properties (size distributions, numbers, etc.) based on statistical evaluations performed on cross-sections through the specimens. Thus a significant fraction of the cut crystals (in the cross-sections) can be smaller than the resolution limit of the microscope used, which may lead to an underestimation of the crystal numbers and, consequently, of the determined values of nucleation rates. In Refs. [25,26], equations were derived for the fractional underestimation, f, of the number of spherical particles per unit volume and of the nucleation rates, as obtained from stereological techniques for reflected light microscopy or SEM, for typical cases of crystal nucleation in glasses. The following two cases bound the most common experimental situations: (i) a monodisperse system of spherical particles that can result from instantaneous heterogeneous nucleation; (ii) a uniform size distribution of spherical particles from the critical size to D_M, where D_M is the largest diameter of the clusters in the distribution. Such distribution is typical for simultaneous nucleation and growth with constant rates in a single-stage heat treatment. The equations for these cases are:

Case (i). Monodisperse systems:

$$f = \frac{2}{\pi}\arcsin(\sigma_1), \tag{15}$$

Case (ii). Uniform size distribution from the critical size to D_M:

$$f = 1 - \left\{\frac{2}{\pi}[\cos\theta_1[1 - \ln(1+\sin\theta_1)] + \theta_1 + \sigma_1\ln\sigma_1 - \sigma_1]\right\}. \tag{16}$$

In above equations, $\theta_1 = \arccos\sigma_1$, $\sigma_1 \equiv \varepsilon/D_M$, and ε is the resolution limit of the microscope used. Comparison with experimental nucleation data for two silicate glasses demonstrated that these equations predict well the observed underestimations of the number of spherical particles. Fig. 2 shows the function f for cases (i) and (ii).

To minimize these errors employing reflected light optical microscopy methods, one should use high magnification objective lenses or SEM. Alternatively, transmission methods could be used because they lead to much smaller errors than reflection techniques.

Similar underestimates occur when one tries to determine volume fractions crystallized, and these may be subjected to significant errors when the largest grain size of the distribution is close to the microscope resolution limit [26]. For transformations occurring from a fixed number of nuclei, the systematic errors are smaller than those observed in the continuous nucleation case, but can still be significant when reflected light microscopy is used. Transmission methods are more time-consuming, but lead to much smaller errors than reflection techniques.

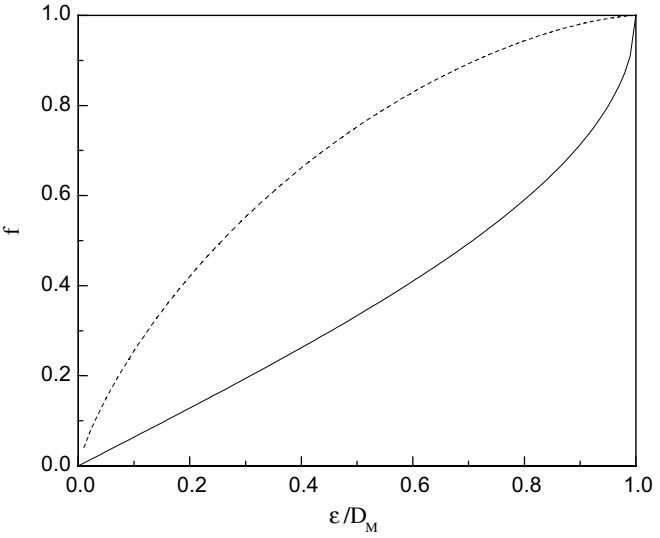

Fig. 2. Fractional underestimation of the number of spherical particles versus the ratio between the microscope resolution limit and the largest particle diameter. Solid and dashed curves refer to cases (i) and (ii), respectively.

3.5. Probabilistic approach for the analysis of the nucleation process

For the sake of completeness we should briefly mention a method based on the stochastic nature of nucleation [27]. The appearance of critical nuclei is a stochastic event that can be characterized by an average waiting period, $\bar{\tau}$,

$$\bar{\tau} = \frac{1}{IV}, \tag{17}$$

where I is the nucleation rate and V is the volume of the system under study.

Since the probability of critical nucleus formation due to a successful series of attachment and separation reactions is very low, nucleation can be treated as a Poissonian process. Hence the probability of appearance of one critical nucleus in a time period τ^1 is

$$P_1(\tau^1) = \lambda\tau^1\exp(-\lambda\tau^1), \tag{18}$$

where $\lambda = 1/\bar{\tau}$.

In cases of high nucleation rates, their measurement is normally limited to relatively low undercoolings that correspond to high values of the crystal growth rate. Thus, the first few super-critical nuclei trigger crystallization of the whole sample. Fitting the experimental distribution of waiting times of the first nucleus, τ^1, to Eq. (18) one can estimate an average waiting period, $\bar{\tau}$, and then the nucleation rate from Eq. (17). Such analysis has been employed, e.g., for metals dispersed in the form of small drops when the use of other methods is connected with difficulties (see, e.g., [13,28]).

3.6. Overall crystallization kinetics

Crystal nucleation followed by subsequent growth results in the overall crystallization of the sample. This

process can be described by determining the volume fraction of the transformed phase, $\alpha(t)$. The formal theory of overall-crystallization kinetics under isothermal conditions was developed in the late 1930s by Kolmogorov [29], Johnson and Mehl [30], and Avrami [31], and is well-known as the JMAK theory. According to this theory, the volume fraction of the new phase is given by

$$\alpha(t) = 1 - \exp\left[-g\int_0^t I(t')\left[\int_{t'}^t U(t'')\,dt''\right]^3 dt'\right], \tag{19}$$

where g is a shape factor, which is equal to $4\pi/3$ for spherical crystals. If the nucleation (I) and growth (U) rates are constant throughout the transformation (e.g., steady-state homogeneous stoichiometric nucleation), Eq. (19) can be rewritten as

$$\alpha(t) = 1 - \exp\left[-\frac{gIU^3t^4}{4}\right]. \tag{20}$$

When the number of growing crystals, N_o, does not change with time (as it is typical for fast heterogeneous nucleation on a finite number of active sites), Eq. (19) transforms to

$$\alpha(t) = 1 - \exp[-gN_oU^3t^3]. \tag{21}$$

Avrami proposed that, in general, the following relation should be used:

$$\alpha(t) = 1 - \exp(-Kt^n). \tag{22}$$

In typical applications, Eq. (22) is employed in the form

$$\ln(-\ln(1-\alpha)) = \ln K + n\ln t. \tag{23}$$

The values of K and n can be estimated then by fitting the experimental data of $\alpha(t)$ to Eq. (23). Thus the coefficient K includes I and U, or N_o and U. The Avrami coefficient, n, depends on both nucleation and growth mechanisms, and can be written for the case of three-dimensional growth as

$$n = k + 3m, \tag{24}$$

where k and m are taken from the formulas $N \sim t^k$ and $r \sim t^m$ describing the variation of crystal number (N) and crystal size (r) with time.

The knowledge of the Avrami coefficient, n, is helpful to understand the mechanism of phase transformation at a given temperature. When it is possible to independently measure the crystal growth rate, one can then calculate the nucleation rate from the coefficient K. This method is not as precise as direct measurements, but can give useful information about nucleation in advanced stages of crystallization, when the application of other methods is hindered (see Section 5).

For the simplest cases of constant nucleation rate (or constant number of crystals) and linear growth, Eqs. (20) and (21) have been tested by using I_{st}, U, and N_o data independently measured by optical microscopy in glasses of stoichiometric compositions $2Na_2O\cdot CaO\cdot 3SiO_2$ [32] and $Na_2O\cdot 2CaO\cdot 3SiO_2$ [33]. Good agreement was obtained between the values of gIU^3 (or gN_oU^3), calculated from fitting the $\alpha(t)$-data to the JMAK equation, and directly measured values. Recently, the JMAK-equation was also successfully employed, together with measured crystal growth rates, to estimate extremely high nucleation rates in a stoichiometric glass of fresnoite composition [34].

4. Interpretation of nucleation experiments by the classical nucleation theory

4.1. Non-steady state (transient) nucleation

4.1.1. Estimation of the time-lag in nucleation

Typical $N(T_n, T_d, t)$-curves obtained by the 'development' method are shown in Fig. 3. As we already mentioned, only the nuclei that achieve the critical size, $r_*(T_d)$, during heat treatment at T_n can grow at the development temperature T_d. The other nuclei have a high probability to dissolve at T_d. As the result, the number of crystals nucleated at given conditions and developed at T_d has, strictly speaking, to decrease with increasing T_d

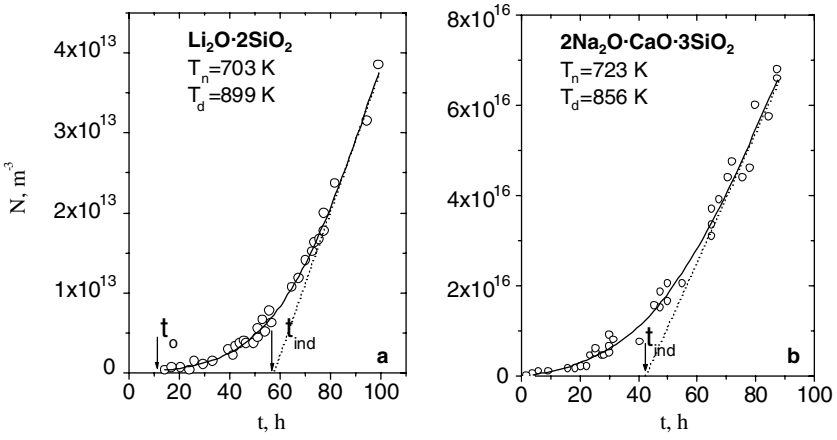

Fig. 3. Typical curves of the number density of $Li_2O\cdot 2SiO_2$ (a) and $2Na_2O\cdot CaO\cdot 3SiO_2$ (b) crystals in glasses of respective stoichiometric compositions versus time of nucleation obtained by the 'development' method [35,36].

(see Figs. 4 and 5). The total number of supercritical crystals, N, nucleated at a temperature, T_n, in a time, t, is given by

$$N(T_n, r_*(T_n), t) = \int_0^t I(T_n, t')\,dt'. \quad (25)$$

The number of crystals nucleated in the same conditions, but having sizes larger than the critical size, $r_*(T_d)$, and which are, consequently, capable to grow at T_d, is given by

$$N(T_n, r_*(T_d), t) = \int_0^{t-t_0} I(T_n, t')\,dt', \quad (26)$$

where t_o is the period of time that critical nuclei of size $r_*(T_n)$ need in their growth to reach the size $r_*(T_d)$. This time interval is determined by

$$t_o(T_n, T_d) = \int_{r_*(T_n)}^{r_*(T_d)} \frac{dr}{U(T_n, r)}. \quad (27)$$

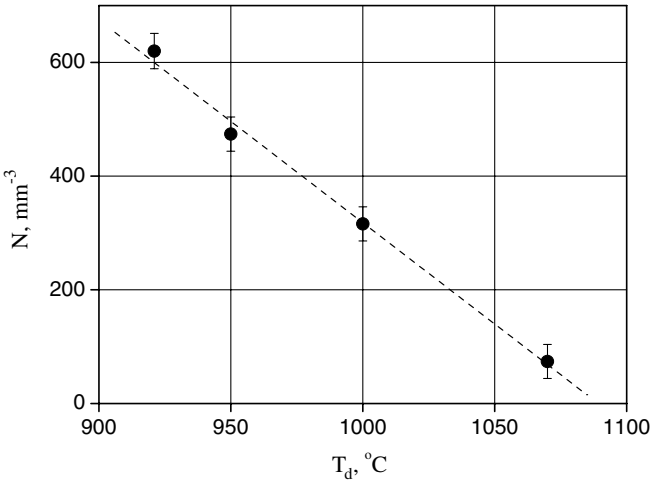

Fig. 4. Number density of crystals versus development temperature in a lithium aluminum silicate glass subjected to nucleation treatment for 5 min at $T_n = 785$ °C [37].

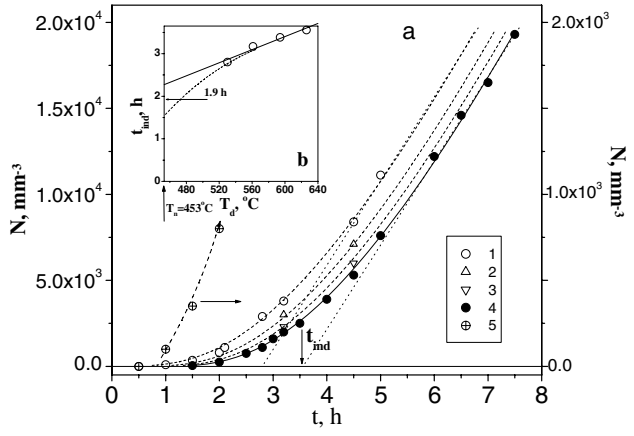

Fig. 5. (a) Number density of $Li_2O{\cdot}2SiO_2$ crystals developed at $T_d = 530$ °C (curves 1 and 5), 560 °C (curve 2), 594 °C (curve 3), and 626 °C (curve 4) as a function of nucleation time at $T_n = 453$ °C [38]. (b) Induction time versus development temperature.

Eqs. (25) and (26) yield

$$N(T_n, r_*(T_n), t) = N(T_n, r_*(T_d), t + t_o). \quad (28)$$

Hence, $N(T_n, r_*(T_n), t)$ plots are similar to $N(T_n, r_*(T_d), t)$-plots with the difference that the latter is shifted along the time-axis by a time t_o. *Thus, the development method can provide the correct value of the steady-state nucleation rate, but overestimates the induction time for nucleation by* t_o.

The period during which heat treatment at the nucleation temperature T_n does not influence crystallization at T_d can be identified with t_o (given by Eq. (27); here we neglect the time of the first critical nucleus formation). This time is indicated by an arrow in Fig. 3(a). According to Eq. (27), the higher the growth rate U at the nucleation temperature, T_n, and the closer is T_d to T_n ($r_*(T_n)$ is correspondingly closer to $r_*(T_d)$), the lower is t_o. Hence, for a strong overlap of the nucleation and growth rate curves, the value of t_o is not very high and can often be neglected. Fig. 3(b) confirms this assumption for a $2Na_2O{\cdot}CaO{\cdot}3SiO_2$ glass. On the other hand, when the overlap of the nucleation and growth rate curves is weak, as observed for lithium disilicate glass, one has to reduce the measured value of $t_{ind}(T_n, T_d)$ by a time $t_o(T_n, T_d)$ (see Fig. 3(a)) to estimate $t_{ind}(T_n)$. The value of $t_{ind}(T_n)$ can be roughly estimated via extrapolation of the $t_{ind}(T_n, T_d)$-values for the $N(T_n, T_d, t)$-curves, obtained at different T_d, to t_{ind} corresponding to $T_d = T_n$. Fig. 5(a) presents examples of such $N(T_n, T_d, t)$-curves for lithium disilicate glass. Fig. 5(b) shows the values of t_{ind}, taken from these curves, versus development temperature. When T_d approaches $T_n = 453$ °C, t_{ind} is about 1.9 h (the average value of the linear and quadratic polynomial extrapolations). Hence, one can approximately estimate t_o as $t_o(T_d, T_n) = t_{ind}(T_n, T_d) - t_{ind}(T_n)$, e.g., for $T_d = 530$ °C and $T_n = 453$ °C t_o is about 0.9 h. A similar value is obtained by extrapolating the initial section of the $N(t)$-curve 1 (see also curve 5) to $N = 0$. Thus, according to Eq. (12), one can assume that Eq. (29) holds, i.e.,

$$\tau(T_n) = \frac{6}{\pi^2}(t_{ind}(T_n, T_d) - t_o(T_n, T_d)). \quad (29)$$

Kinetic $N(t)$-curves, such as those presented by Fig. 3, can be plotted in dimensionless coordinates $(N(T, t - t_o)/I_{st}(T)\tau(T)$ versus $(t - t_o)/\tau(T))$. Fig. 6(a) shows that these coordinates allow one the combination of data for different glasses and different temperatures in the same plot. The experimental points are quite close to the theoretical master curve calculated with Eq. (10). This curve corresponds to increasingly higher nucleation rates towards the steady-state value, I_{st}. The evolution of the nucleation rate calculated by Eq. (9) is shown in Fig. 6(b).

As we already mentioned in Section 3.3, if one employs the single-stage method, the induction periods obtained from experimental $N(T_n, t)$-curves must be reduced by a period of time $t_o \approx r_{res}/U(T_n)$. An example of such curve, obtained for Au-catalyzed nucleation in $NaPO_3$ glass, is

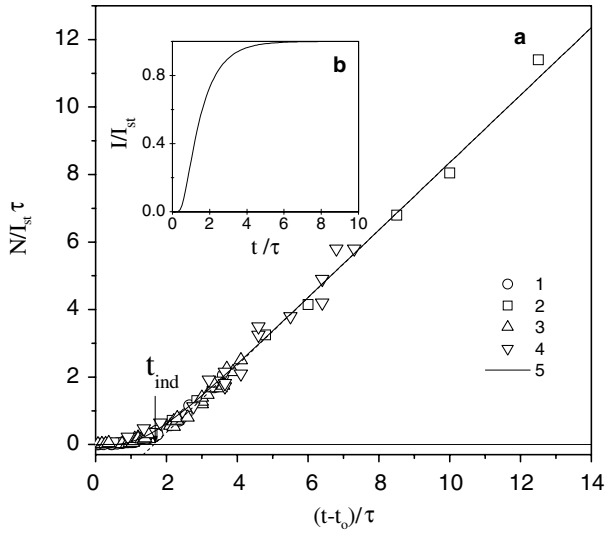

Fig. 6. (a) $N/(I_{st}\tau)$ versus reduced time for glasses $Li_2O{\cdot}2SiO_2$ (curves 1 and 2), and $2Na_2O{\cdot}CaO{\cdot}3SiO_2$ (curves 3 and 4) [35] for $T = 430$ °C (curve 1), 465 °C (curve 2), 465 °C (curve 3) and 470 °C (curve 4). Curve 5 was calculated from Eq. (10). (b) Reduced nucleation rate versus reduced time calculated from Eq. (9).

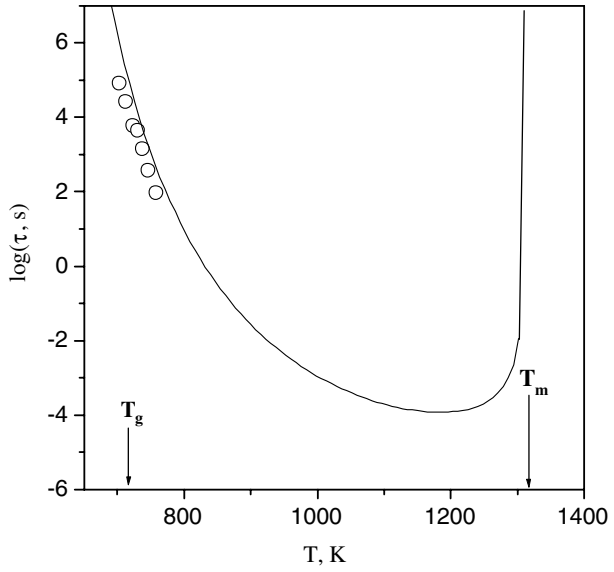

Fig. 8. Temperature dependence of the time-lag for nucleation. Circles refer to experimental data for $Li_2O{\cdot}2SiO_2$ glass [41]. The full line was calculated by Eq. (8).

shown in Fig. 7. The dashed line indicates the case of steady-state nucleation where the shift, t_o, is taken into account. The comparison of this line with experimental data gives clear evidence for the transient character of the $N(t)$-curves. It should be emphasized that one of the first experimental demonstrations of transient nucleation in glasses was presented in Ref. [39].

4.1.2. Temperature dependence of the time-lag for nucleation

According to Eq. (8), when the degree of undercooling increases, the time-lag τ passes through a minimum. This behavior is due to the interplay between the decrease of $1/\Delta G_V^2$ and the increase of the exponential term. This minimum is located at a low undercooling. Since, in the case of glass-forming silicate melts, detectable (internal) homogeneous nucleation rates are observed only at very deep undercoolings, $\Delta T/T_m \geqslant 0.4$ [40], at these undercoolings only an increase of the time-lag with increasing undercooling is observed. Fig. 8 illustrates this trend for lithium disilicate glass. The circles refer to experimental data. The solid line is determined according to Eq. (8) with $\sigma_{cm} = 0.2$ J/m^2 assuming that the activation free energy ΔG_D is equal to that for viscous flow, ΔG_η. For deep undercoolings the validity of this last assumption has been a subject of controversial discussion, however, it is commonly assumed to be valid for $T > 1.2T_g$ (see, e.g., [42]).

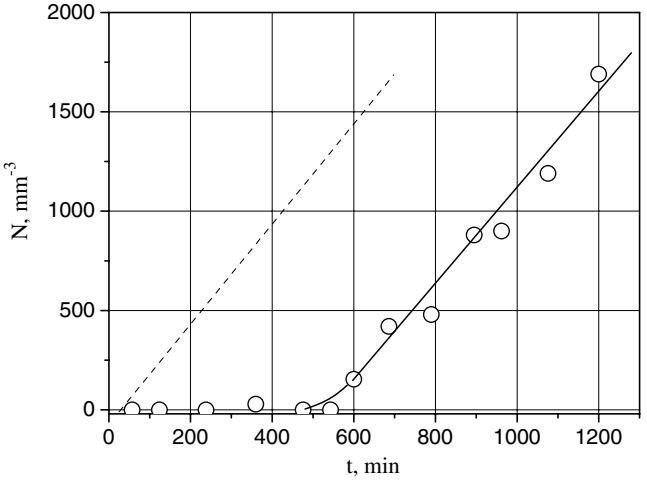

Fig. 7. Number density of crystals in $NaPO_3$ glass doped with 0.45% Au versus time of heat treatment at $T = 332$ °C obtained by a single-stage method [39]. The dashed line refers to the steady-state nucleation rate. The shift due to the time required to grow the crystals to visible sizes is taken into account.

4.1.3. Transient nucleation with a pre-existing nucleus size distribution

So far we discussed transient nucleation assuming the absence of an appreciable number of pre-existing nuclei. This assumption is quite reasonable for interpreting time-lag phenomena for glasses obtained via fast quenching of the melt. In contrast, preliminary annealing of a glass at some temperature, T_1, for sufficiently long times, $t \geqslant \tau(T_1)$, results in the formation of a cluster distribution that acts as an initial distribution at the temperature T_2. Then this distribution evolves towards a steady-state distribution corresponding to the temperature T_2, *complicating* the time-dependence of the nucleation rate.

For example, for lithium disilicate glass annealed at T_1, the nucleation rate at $T_2 > T_1$ passes through a maximum before reaching the steady-state value. Fig. 9 shows the $N(t)$-curves at $T_2 = 465$ °C for a rapidly quenched parent glass (curve 1) and for glasses that had been previously annealed at $T_1 = 430$ °C (curves 2 and 3). All curves were

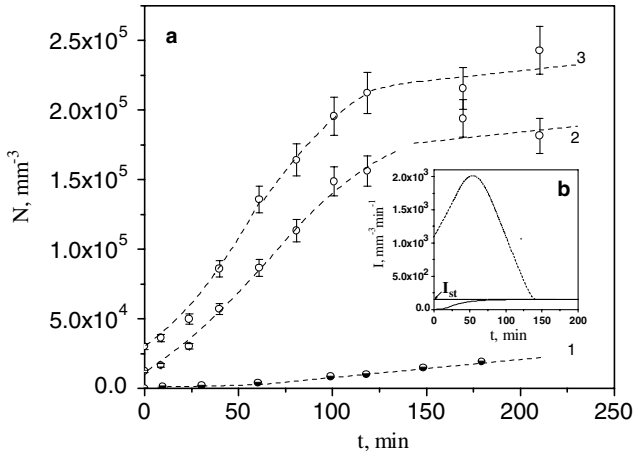

Fig. 9. (a) Number density of $Li_2O{\cdot}2SiO_2$ crystals obtained via the 'development' method ($T_d = 626$ °C) versus time of nucleation at $T_n = 465$ °C. Curve 1 refers to the quenched glass. Curves 2 and 3 refer to glasses subjected to preliminary treatment at $T = 430$ °C for 65 h (curve 2) and 89 h (curve 3) [43]. (b) Nucleation rate versus time. Solid and dashed lines correspond to curves 1 and 3 from (a), respectively.

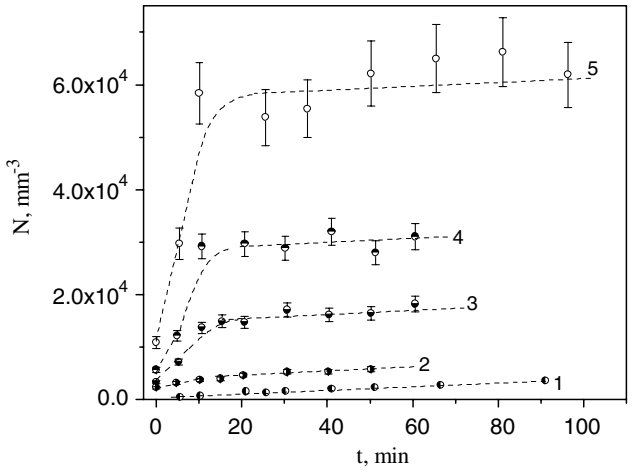

Fig. 10. Number density of $Li_2O{\cdot}2SiO_2$ crystals obtained via the 'development' method ($T_d = 626$ °C) versus time of nucleation at $T_n = 485$ °C. Curve 1 quenched glass, curves 2–5 glasses subjected to preliminary treatment at $T = 473$ °C (curve 2), 451 °C (curve 3), 440 °C (curve 4), and 430 °C (curve 5) for the following times: $t = 0.75$ h (curve 2), 4.5 h (curve 3), 18 h (curve 4), and 65 h (curve 5) which exceed the time-lags at T [43].

obtained by the 'development' method at $T_d = 626$ °C. Curves 2 and 3 demonstrate, as compared with curve 1, a strong increase in the number of crystals, and only for times higher than about 120 min the nucleation rate reaches steady-state conditions corresponding to the temperature T_2. The evolution of the nucleation rate corresponding to curve 3 is shown in Fig. 9(b).

Such unusual behavior of the nucleation kinetics is caused by the transition of an initial distribution formed at T_1 for sizes less than $r_*(T_d)$ into the steady state cluster size distribution corresponding to T_2. Since the number of nuclei having sizes $r \geqslant r_*(T)$ increases with decreasing temperature, down to $T = T_m/3$, a strengthening of the effect of the preliminary heat treatment with decrease of T_1 should be expected. This is indeed the case as shown in Fig. 10. The presented effects of the multistage heat treatments were well-described by the numerical modeling of the cluster evolution performed in the framework of the classical nucleation theory [44–46] with the exception of the heat treatments involving the temperature $T_1 = 430$ °C [45]. Since the values of the parameters needed for the simulations were estimated via a fitting procedure this disagreement could be caused by the error in the $I_{st}(430\ °C)$ estimation or viscosity data taken from other authors. Nevertheless, the simulations clearly show that the nucleation kinetics is governed by the evolution of the nuclei distribution.

4.2. Steady-state nucleation

4.2.1. Temperature dependence of steady-state nucleation rates

Some examples of steady-state nucleation rates, I_{st}, measured from the slope of the linear part of the $N(t)$-plots, such as those shown in Fig. 3, are presented in Fig. 11 as a function of reduced temperature. The values of $I_{st}(T)$

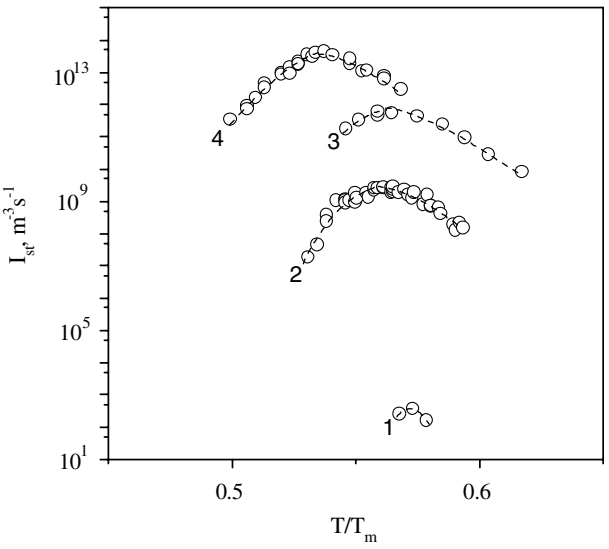

Fig. 11. Steady-state nucleation rate versus reduced temperature for some stoichiometric glasses: (curve 1) $3MgO{\cdot}Al_2O_3{\cdot}3SiO_2$ [47]; (curve 2) $Li_2O{\cdot}2SiO_2$ [35]; (curve 3) $Na_2O{\cdot}2CaO{\cdot}3SiO_2$ [48]; (curve 4) $2Na_2O{\cdot}CaO{\cdot}3SiO_2$ [36].

pass through a maximum at a temperature T_{max}. The magnitudes of $I_{st}(T_{max}) \equiv I_{max}$ vary from 5×10^{13} to 3×10^2 m^{-3} s^{-1} and cover practically the whole range of available measurements of nucleation rates in silicate glasses with stoichiometric compositions.

The reason for the existence of the nucleation rate maximum follows from a simple analysis of Eq. (1). Since the pre-exponential term, I_o, depends only weakly on temperature, the temperature dependence of the nucleation rate is determined mainly by the thermodynamic and kinetic barriers for nucleation. A temperature decrease produces two

effects: a decrease of the thermodynamic barrier due to an increase in the thermodynamic driving force for crystallization, leading to a higher nucleation rate, and an increase of the kinetic barrier, leading to a lower nucleation rate (the kinetic barrier is, as mentioned earlier, often replaced by the activation free energy for viscous flow). As a result of these two opposite tendencies, one finds a maximum of the steady-state nucleation rate at a temperature T_{max}, which is located well below T_m.

Eq. (4) for the thermodynamic barrier can be rewritten as

$$\frac{W_*}{k_B T} = C_1 \frac{1}{T_r (1 - T_r)^2}, \quad C_1 = \frac{16\pi}{3} \frac{\alpha_{ST}^3 \Delta H_m}{R T_m}, \quad T_r \equiv \frac{T}{T_m}. \tag{30}$$

Here we used the linear approximation for the thermodynamic driving force, Eq. (6), and the following semi-empirical equation:

$$\sigma_{cm} = \alpha_{ST} \frac{\Delta H_m}{V_m^{2/3} N_A^{1/3}} \tag{31}$$

for the specific surface energy of the nucleus/melt interface proposed by Skapski and Turnbull [49,50]. In Eq. (31), ΔH_m is the melting enthalpy per mole, V_m is the molar volume, N_A is Avogadro's number, and α_{ST} is an empirical dimensionless coefficient, smaller than unity, reflecting the fact that surface atoms have less neighbors than bulk atoms. Assuming that ΔG_D is of the same order of magnitude as the activation free energy for viscous flow, ΔG_η, one can write the kinetic barrier as

$$\frac{\Delta G_D(T)}{k_B T} = \frac{C_2}{T_r - T_{or}}, \quad C_2 \equiv \frac{2.30B}{T_m} \cong 30(T_{gr} - T_{or}),$$
$$T_{or} \equiv \frac{T_o}{T_m}, \quad T_{gr} \equiv \frac{T_g}{T_m}, \tag{32}$$

where T_o and B are the empirical coefficients of the Vogel–Fulcher–Tammann (VFT) equation and T_g is the glass transition temperature. The application of the VFT-relation implies the assumption of a temperature-dependent activation free energy, ΔG_η. In the definition of C_2 we took into account the fact that $\Delta G_\eta/(k_B T) \cong 30$ at $T = T_g$.

Fig. 12 shows $I_{st}(T_r)$-curves calculated with Eqs. (1), (30), and (32), reasonable estimates of the pre-exponential term and values of the parameters C_1 and C_2, as indicated in the figure caption. One can see that the decrease in the kinetic barrier, caused by a decrease in C_2 at a fixed value of C_1, results in a shift of the nucleation rate maximum to lower temperatures (cf. curves 1–4). The reduced temperature $T_r \equiv T/T_m = 1/3$ is a lower limit to $T_r^{max} \equiv T_{max}/T_m$ obtained when the kinetic barrier tends to zero (cf. curve 5). This shift is accompanied by a strong increase in the magnitude of $I(T_{max}) \equiv I_{max}$. When the thermodynamic barrier is diminished, at fixed values of C_2, by decreasing the parameter C_1 (which is proportional to α_{ST} and the reduced melting enthalpy $\Delta H_m^r = \Delta H_m/RT_m$), the value of I_{max} also increases (curves 1 and 6–8), but the value of T_{max} shifts to higher temperatures.

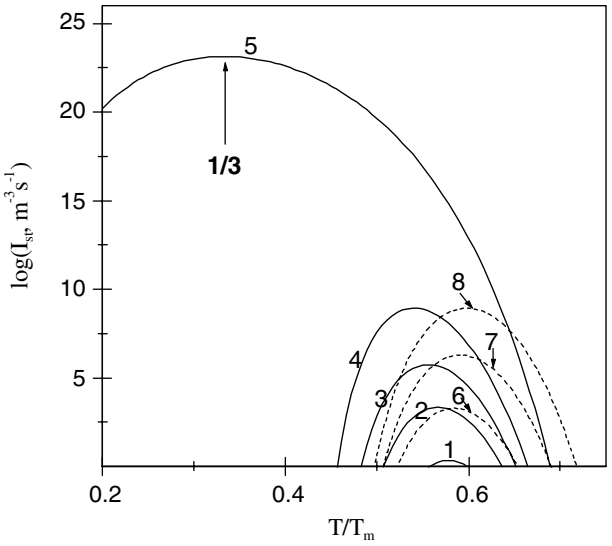

Fig. 12. Temperature dependence of homogeneous nucleation rates. The curves were calculated with Eqs. (1), (30), and (32) with a pre-exponential term $I_o = 10^{42}$ m^{-3} s^{-1} and following values of the parameters characterizing the temperature independent parts of the thermodynamic (C_1) and kinetic (C_2) barriers: $C_1 = 6.5$ (curves 1–5), 5.8 (curve 6), 5.1 (curve 7), 4.5 (curve 8); $C_2 = 6$ (curves 1 and 6–8), 4.8 (curve 2), 3.9 (curve 3), 2.8 (curve 4), 0 (curve 5).

The effect of variation of the kinetic barrier on the nucleation rate can be qualitatively illustrated for lithium disilicate [51] and sodium metasilicate [52] glasses with different H_2O content (a few percent of water often result in a significant decrease of viscosity) as shown in Fig. 13. A decrease in the thermodynamic barrier can be also caused by a decrease in the effective crystal/melt interfacial energy as in the case of heterogeneous nucleation. As a result, as was shown in Ref. [53], the temperature T_{max} for heterogeneous surface nucleation is displaced to higher values as compared with homogeneous nucleation.

4.3. Correlation between nucleation rate and glass transition temperature

The methods discussed in Section 3 to measure nucleation kinetics are both difficult to perform and time consuming. Also, owing to several restrictions, they cannot always be employed. Hence, the knowledge of any correlation between nucleation rate and easily measurable properties of glasses is highly desirable. As one example, well before the development of nucleation theory for condensed systems, Tammann called attention to the following tendency: the higher the melt viscosity at the melting temperature, the lower is its crystallizability [54].

Almost eighty years after Tammann's pioneering research work, James [55] and Zanotto [56], based on numerous experimental nucleation rate data for several silicate glasses, concluded that *glasses having a reduced glass transition temperature, $T_{gr} \equiv T_g/T_m$, higher than*

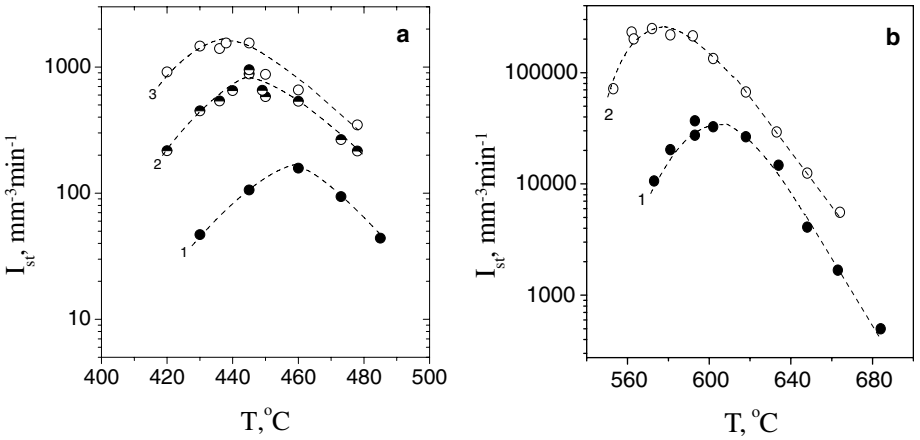

Fig. 13. Temperature dependencies of the steady-state nucleation rates in $Li_2O \cdot 2SiO_2$ [51] (a) and $Na_2O \cdot 2CaO \cdot 3SiO_2$ [52] (b) glasses containing different amounts of H_2O: (a) 0.05 mol% (curve 1), 0.12 mol% (curve 2), and 0.20 mol% (curve 3); (b) 0.01 mol% (curve 1), 0.2 mol% (curve 2).

~0.58–0.60, *display only surface* (*mostly heterogeneous*) *crystallization*; *while glasses showing volume* (*homogeneous*) *nucleation have values* $T_{gr} < 0.58$–0.60. Since at temperatures $T < T_m$ the nucleation rate is always positive, the absence of volume nucleation for glasses having $T_{gr} > 0.60$ merely indicates undetectable nucleation on laboratory time/size scales. Hence, an increase in the nucleation rate with decreasing T_{gr} could be expected. Indeed, a drastic increase of the magnitude of I_{max} with decreasing T_{gr} has been demonstrated by Deubener [57]. Fig. 14 presents a plot of the $I_{max}(T_{gr})$-dependence, which has been extended in Ref. [58] and in the present work. In a relatively narrow range of T_{gr} (from 0.47 to 0.58) shown by 55 glasses of stoichiometric and non-stoichiometric compositions, belonging to eight different silicate systems, *the nucleation rates drop by about* 17 *orders of magnitude*! When

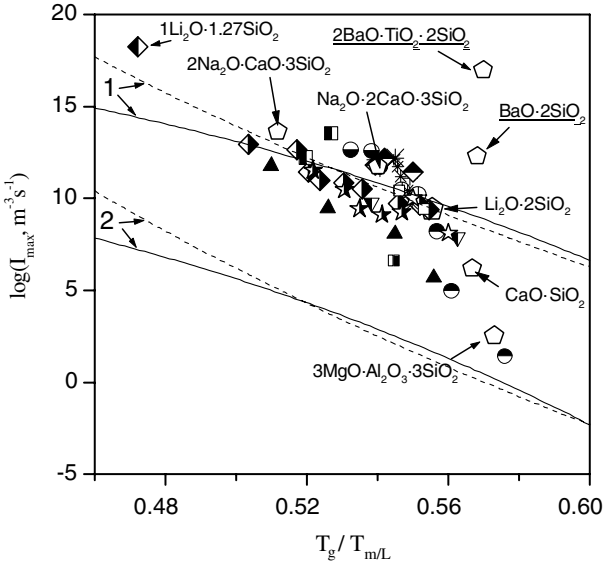

Fig. 14. Maximum nucleation rate as a function of reduced glass transition temperature for 55 silicate glasses. The lines are calculated from CNT with $C_1 = 4.5$ (curves 1) and 6.5 (curves 3). Solid lines refer to $C_2 = 4.5$ and $T_{or} = T_{gr} - C_2/30$; dashed lines to $T_{or} = 0.4$ [58].

T_{gr} increases, the kinetic inhibition of nucleation proceeds at higher temperatures and at higher values of the thermodynamic barrier due to lower values of the thermodynamic driving force. As a consequence, nucleation becomes practically undetectable at $T_{gr} > 0.58$. This result confirms the findings of James [55] and Zanotto [56]. The lines in Fig. 14 are calculated from CNT (Eqs. (1), (30), and (32)) with reasonable values of the parameters C_1 and C_2 indicated in the figure caption. Remember that C_1 and C_2 characterize the temperature independent parts of the thermodynamic and kinetic barriers for nucleation, respectively. Since Eq. (32) contains two independent parameters C_2 and T_{or}, the viscosity and, correspondingly, T_{gr}, was varied in two different ways, by keeping either C_2 (solid line) or T_{or} (dashed line) fixed. In the most interesting temperature range ($0.5 < T_r < 0.6$) these different ways of varying T_{gr} lead to similar results. The lines reflect correctly the experimentally observed general trend. However, in applying the mentioned rule to particular systems one has to act with some precaution since a substantial variation of the thermodynamic barrier can result in a considerable variation of I_{max} for glasses having similar values of T_{gr}. For instance, fresnoite ($2BaO \cdot TiO_2 \cdot 2SiO_2$) and wollastonite ($CaO \cdot SiO_2$) glasses have T_{gr} about 0.57, while the values of the parameter α_{ST} are 0.4 and 0.6, respectively. The latter fact leads to a strong difference in the values of the thermodynamic barriers and correspondingly to a strong difference in I_{max}. Also nucleation of metastable phases, such as $BaO \cdot 2SiO_2$, is possible as shown in Ref. [59].

An important parameter is the location of T_{max}. It is commonly accepted that T_{max} is close to T_g. However, it was shown in Ref. [58] that the ratio T_{max}/T_g depends on T_{gr}. T_{max}/T_g is higher than one (i.e., T_{max} exceeds T_g) at low T_{gr}, approaches one at about $T_{gr} \sim 0.55$, and then becomes smaller than one. This trend results in an additional increase of the kinetic barrier at T_{max} with increasing T_{gr} caused by the increase of $\eta(T_{max})$.

Computations of $I_{st}(T)$ temperature dependencies similar to those published in Ref. [58] and presented here were

performed by Turnbull in the 1960s (see, e.g., Ref. [60]). However, at that time, with the exception of the measurements of Tammann [61] and Mikhnevich [62] for organic liquids, nucleation rate data were not available in wide temperature ranges including T_{max}. In order to verify the existence of a correlation between I_{max} and T_{gr}, as proposed here, an abundance of experimental points must be available. This is now the case (cf. Fig. 14).

5. Nucleation rate data and CNT: some serious problems

5.1. Different approaches for the interpretation of experimental data by CNT

As shown in the previous sections, in its original form CNT provides a good qualitative description of nucleation rate data for silicate glasses, however, serious problems arise when one tries to employ this theory for a quantitative interpretation of experimental data.

If one uses the Stokes–Einstein equation to connect the kinetic barrier of nucleation with the glass viscosity one can rewrite Eq. (1) for the steady-state nucleation rate as

$$I_{st} = K_\eta \frac{1}{\eta} \exp\left(-\frac{W_*}{k_B T}\right), \quad K_\eta = I_o \frac{h}{4l^3}, \tag{33}$$

where the size parameter l has the order of the Si–O bond length. Hereby, the diffusivity across the crystal/liquid interface is replaced by the volume diffusivity.

The use of the Stokes–Einstein equation in Eq. (33) can be avoided if one estimates the kinetic barrier from the nucleation time-lag. In this case, Eq. (1) takes the following form:

$$I_{st} = K_\tau \frac{1}{\Delta G_V^2 t_{ind}} \exp\left(-\frac{W_*}{k_B T}\right), \quad K_\tau = I_o \frac{8h\sigma_{cm}}{3a^4}. \tag{34}$$

In the analysis of crystallization kinetics in glass-forming systems, it is commonly accepted – in accordance with CNT and Gibbs' classical description of heterogeneous systems – to use the properties of the newly evolving macrophase as reference states for the description of the bulk properties of the critical nucleus. Additionally one has to properly specify the value of the specific interfacial energy, σ_{cm}. Since measurements of the interfacial energy of the crystals in their own melt are confronted with serious difficulties, one usually employs the easily measurable thermodynamic driving force for crystallization of the macrophase for the determination of the work of critical cluster formation. Hereby, σ_{cm} is commonly taken as a fit parameter and is treated, to a first approximation, as a size-independent (capillarity approximation) and temperature independent quantity. The respective values of σ_{cm} are denoted in Tables 1 and 2 as σ^*_{cm}. These approximations allow one to estimate both the magnitude of the pre-exponential term, I_o, in Eq. (1) and the value of crystal-melt surface energy, σ_{cm}, from a fit of experimental data (I_{st}, η, or t_{ind}). According to Eqs. (33), (34), and (4), $\ln(I_{st}\eta)$ and $\ln(I_{st}t_{ind}\Delta G_V^2)$ versus $1/(T\Delta G_V^2)$ plots should yield straight lines. Their intercepts and slopes can be employed to evaluate I_o and σ^*_{cm}, respectively. However, these approximations lead to the following problems:

Table 1
Ratio of experimental and theoretical pre-exponential, and surface energy values calculated by CNT for different glasses [40]

Glass	$\Delta C_p = 0$		$\Delta C_p = f(T)$	
	$\log(I_o^{exp}/I_o^{theo})$	σ^*_{cm}	$\log(I_o^{exp}/I_o^{theo})$	σ^*_{cm}
$Li_2O{\cdot}2SiO_2$	15	0.19	19	0.20
$Na_2O{\cdot}2CaO{\cdot}3SiO_2$	18	0.17	72	0.19
$2Na_2O{\cdot}CaO{\cdot}3SiO_2$	27	0.15	139	0.17

The specific interfacial energy is given in J m^{-2}.

Table 2
Liquid–crystal surface energies (in J m^{-2}) calculated from nucleation and growth data [69]

Glass	σ_{cm}	σ^*_{cm}	σ^{**}_{cm}	K	σ^r_{cm}
$Li_2O{\cdot}2SiO_2$	1.4	0.20	0.152–0.156 (450 °C < T < 485 °C)	0.19–0.23	0.050–0.060
$Na_2O{\cdot}2CaO{\cdot}3SiO_2$	1.5	0.18	0.099–0.110 (580 °C < T < 685 °C)	0.13	0.026

(i) The use of Eq. (33) [55,63] and Eq. (34) [64] leads to drastic discrepancies between the experimental, I_o^{exp}, and theoretical, I_o^{theo}, values of the pre-exponential factor. This discrepancy was first observed for crystal nucleation in undercooled Ga [65] and Hg [66]. In order to illustrate this issue, Table 1 shows the (I_o^{exp}/I_o^{theo})-ratio, and surface energy values for some stoichiometric silicate glasses calculated from $\ln(I_{st}t_{ind}\Delta G_V^2)$ versus $1/(T\Delta G_V^2)$ plots for temperatures above the glass transition range. To trace these plots, both the linear (Turnbull) approximation (Eq. (6)) and the experimental values (Eq. (5)) of the thermodynamic driving force for crystallization of the stable macro-phases were used. The discrepancy between theory and experiment is strongly affected by the choice of ΔG_V (see also Appendix A, where an analysis similar to that given in Ref. [13] is performed). The experimental values of ΔG_V are close to Turnbull's approximation in the case of $Li_2O{\cdot}2SiO_2$ glass, and to Hoffman's approximation in the case of $2Na_2O{\cdot}1CaO{\cdot}3SiO_2$ glass. These equations normally bound the experimental values of ΔG_V [13], and the (I_o^{exp}/I_o^{theo})-ratio increases as one passes from Turnbull's to Hoffman's approximation. However, independently of the particular choice of the expression of the thermodynamic driving force, i.e., with any reasonable approximation or with experimental values of ΔG_V, the mentioned *discrepancy remains quite large*.

(ii) The values of the surface energy, σ_{cm}, calculated as described above (in the deeply undercooled regime close to T_g), are lower than the melt–vapor surface energy, σ_{mv}, which can be measured directly [67,68] (above the equilibrium melting point) by a factor of about 0.5–0.6. These values must then be corrected since σ_{cm} refers to nuclei of critical size, r_*, while σ_{mv} refers to planar melt/vapor interfaces. In the case of lithium disilicate glass, for instance, corrections made with the Tolman equation, Eq. (35), for the size effect, increase this factor to 0.8 [69]. Such high values of σ_{cm}, as compared with σ_{mv}, strongly overestimate its real magnitude. Indeed, according to Stefan's rule [70], one would expect the ratio σ_{cm}/σ_{mv} to be approximately equal to $\sigma_{cm}/\sigma_{mv} \cong \Delta H_{cm}/\Delta H_{mv} \ll 1$, where $\Delta H_{cm} \equiv \Delta H_m$ and ΔH_{mv} are the melting enthalpy of the crystalline phase and enthalpy of evaporation, respectively.

It follows that the widespread believe – the driving force of critical cluster formation can be determined correctly via the classical Gibbs' approach and all necessary corrections have to be incorporated into the theoretical description via the introduction of appropriate values of the specific interfacial energy – is challenged by above given analysis and has to be reconsidered. In the following sections, possible reasons for the failure of CNT in application to a quantitative description of nucleation experiments will be analyzed in detail.

5.2. Temperature and size-dependence of the nucleus/liquid specific surface energy

The discrepancy between experimental and theoretical values of I_o can be avoided if one calculates σ_{cm} from nucleation data (I_{st} and t_{ind} or η) employing the theoretical expression for I_o. This procedure slightly decreases the values of σ_{cm} and leads to a weak increase of σ_{cm} with increasing temperature [71] ($d\sigma/dT \sim (0.06\text{–}0.16) \times 10^{-3}$ J/m^2 K) regardless of the way of estimating the kinetic barrier. As far as we know, Turnbull [66] was the first to draw attention to this fact. At a first sight such kind of temperature dependence of σ_{cm} (i.e., an increase of the surface tension with increasing temperature obtained via the mentioned treatment of nucleation experiments) is in conflict with the theoretical expectations of most, but not all, authors (see the discussion below). Commonly the opinion is favored that, from a thermodynamic point of view, a *decrease* of σ_{cm} (for planar interfaces (σ_∞)) with temperature should be expected [72–74], at least, in the temperature range where crystallization processes may occur [74]. It follows that we are confronted here with a contradiction between the discussed interpretation of experimental results and general theoretical expectations.

As will be shown now this contradiction can be partly removed by taking into account a possible curvature (or nucleus size) dependence of the surface energy. Recall that the specific surface energy estimated from nucleation rate data refers to nuclei of critical size. Curvature corrections are expected to reduce the effective value of the surface energy. When the critical nucleus size increases with increasing temperature, the effect of curvature corrections decreases (see Eq. (35)), leading to higher effective values of the surface energy.

To a first approximation, Tolman's equation (that was originally derived for a liquid drop in equilibrium with its vapor) can be used to decouple these size and temperature effects. The Tolman equation reads

$$\sigma(r_*) = \frac{\sigma_\infty}{\left(1 + \frac{2\delta}{r_*}\right)}, \tag{35}$$

where the Tolman parameter δ is a measure of the (unknown) width of the interfacial region between the coexisting phases.

Employing this relation, the work of formation of a spherical critical nucleus may be written as

$$W_* = \frac{16\pi}{3} \frac{\sigma_\infty^3}{\left(1 + \frac{2\delta}{r_*}\right)^3 \Delta G_V^2}, \tag{36}$$

where

$$r_* = \frac{2\sigma_\infty}{\Delta G_V} - 2\delta \tag{37}$$

holds.

Fig. 15 shows the average values of $(d\sigma_\infty/dT)$ at $T \geqslant T_g$ versus the Tolman parameter. Using experimental nucleation data for $Li_2O \cdot 2SiO_2$ glass, fits of σ_∞ have been performed for different values of δ employing Eq. (34). For this glass, as δ increases $(d\sigma_\infty/dT)$ progressively decreases and becomes negative for $\delta > 2.4 \times 10^{-10}$ m. Thus, reasonable values of the Tolman parameter may be chosen such that σ_∞ *decreases with increasing temperature*, in line with

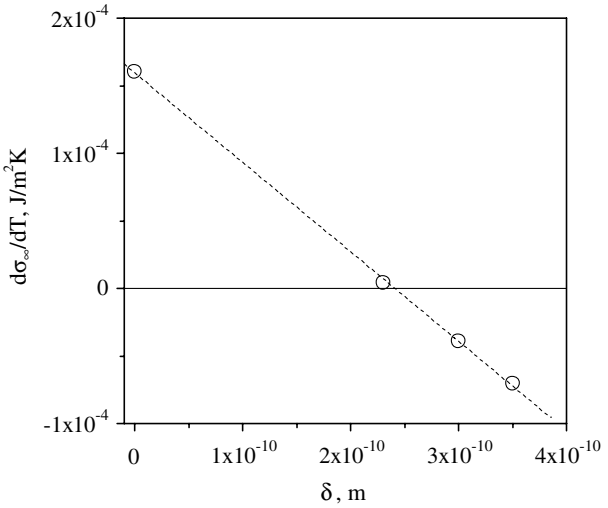

Fig. 15. $(d\sigma_\infty/dT)$ versus Tolman's parameter for $Li_2O \cdot 2SiO_2$ crystals in a glass of the same composition. The kinetic barrier for nucleation was estimated from the nucleation time-lag.

the theoretical predictions of Refs. [72,73]. Similar results were obtained for a $Na_2O{\cdot}2CaO{\cdot}3SiO_2$ glass [71].

For completeness of the discussion, we would like to mention also another interpretation of the increase of σ_{cm} with increasing temperature widely discussed in Ref. [75]. The argumentation is based on model considerations supposing an increased ordering of the liquid near the crystal. These ideas were expressed first by Turnbull [66] and result in an entropy decrease. Employing some plausible assumptions, the positive temperature coefficient of σ_{cm} can be accounted for then by the mentioned entropy loss. Running ahead we could also suppose that the temperature dependence of σ_{cm} is the result of a possible change of the critical nucleus composition and/or structure with its size.

However, regardless of the above possible interpretations the values of the specific surface energy estimated from nucleation rate data in the framework of the classical Gibbs' approach remain too high when compared with the respective melt–vapor surface energies. Consequently, the problem posed at the end of the preceding section remains unsolved by these considerations.

5.3. Estimation of crystal/liquid specific surface energies via dissolution of subcritical nuclei

Essentially all known methods to determine the nucleus-undercooled liquid surface energy are based on nucleation experiments involving certain additional assumptions. However, in order to test the classical nucleation theory or to make theoretical predictions, independent estimates of the specific surface energy are required. Such an independent method of estimating σ_{cm} for clusters of near-critical sizes has been developed recently [69]. The results are summarized below.

The new method is based on the dissolution phenomenon (discussed in Sections 3 and 4) of subcritical nuclei with an increase in temperature. As we already have shown, an $N(T_n, r_*(T_n), t)$-plot coincides with the $N(T_n, r_*(T_d), t)$-plot, with the only difference that the latter is shifted along the time-axis by a time t_o (Eq. (27)). Then, kinetic $N(T_n, t)$-curves obtained with different development temperatures T_{d1} and $T_{d2} > T_{d1}$ should be shifted with respect to each other by a time $\Delta t_o = t_{o2} - t_{o1}$. Fig. 5 shows an example of such kinetic curves. The following equation:

$$\Delta t_o = \int_{r_*(T_{d1})}^{r_*(T_{d2})} \frac{dr}{U(T_n, r)} = \frac{1}{U(T_n, \infty)} \left[r_*(T_{d2}) - r_*(T_{d1}) + r_*(T_n) \ln \left(\frac{r_*(T_{d2}) - r_*(T_n)}{r_*(T_{d1}) - r_*(T_n)} \right) \right] \tag{38}$$

was derived in Ref. [38] to estimate this shift. In the derivation of Eq. (38) a size-dependent crystal growth velocity [76] was used of the form

$$U(T, r) = U(T, \infty) \left[1 - \frac{r_*(T)}{r} \right]. \tag{39}$$

Employing Eq. (3) for the critical nucleus size and assuming that σ_{cm} depends only slightly on temperature, Eq. (38) can be rewritten as

$$\sigma_{cm} = \frac{1}{2} \frac{\Delta t_o U(T_n, \infty)}{\left[\frac{1}{\Delta G_V(T_{d2})} - \frac{1}{\Delta G_V(T_{d1})} + \frac{1}{\Delta G_V(T_n)} \ln \left[\frac{\frac{1}{\Delta G_V(T_{d2})} - \frac{1}{\Delta G_V(T_n)}}{\frac{1}{\Delta G_V(T_{d1})} - \frac{1}{\Delta G_V(T_n)}} \right] \right]} \tag{40}$$

Hence, it is possible to calculate the average value of σ_{cm} in the temperature range T_n–T_{d2} from experimental values of Δt_o, $U(T_n, \infty)$ and ΔG_V. *Note that in doing so neither nucleation rate nor time-lag data are required.* The values of σ_{cm} calculated by this method for $Li_2O{\cdot}2SiO_2$ and $Na_2O{\cdot}2CaO{\cdot}3SiO_2$ glasses are collected in Table 2, which also shows values estimated with the assumption of a size and temperature independent specific surface energy, σ^*_{cm} (see also Table 1) and σ^{**}_{cm} employing the theoretical values of I_o. The values of σ_{cm} calculated via Eq. (40) significantly exceed the corresponding values calculated from a fit of nucleation rate data to CNT (σ^*_{cm}, σ^{**}_{cm}). According to CNT such high values of σ_{cm} lead to vanishing nucleation rates. However, nucleation processes do occur and are indeed observed in deeply undercooled glasses!

In order to find out the origin of this discrepancy, one should realize that the methods discussed above do not provide us with the surface energy directly, but instead only give its combination with the thermodynamic driving force. In particular, σ_{cm} is calculated from the measured values of Δt_o and $U(T_n, \infty)$ via (see Eq. (40))

$$\Delta t_o = \frac{2}{U} \sigma_{cm} f\left(\frac{1}{\Delta G_V} \right) \tag{41}$$

and σ^{**}_{cm} (as well as σ^*_{cm}) from the thermodynamic barrier for nucleation

$$W_* \sim \frac{(\sigma^{**}_{cm})^3}{\Delta G_V^2}. \tag{42}$$

One should recall again that, in line with Gibbs' thermodynamic description of heterogeneous systems, the thermodynamic driving force for crystallization of macro-crystals has been used to estimate the surface energy of critical and near-critical nuclei. Provided, this assumption is correct then we obtain correct values of the specific interfacial energy. However, if this assumption occurs to be incorrect then also the estimates of the surface energy are not correct. In such case, in order to arrive at correct values of the work of critical cluster formation for nucleation, the value of the surface energy has to be chosen appropriately becoming merely a fit parameter. Hence, the above discussed discrepancy may result from the difference between the macroscopic values of the thermodynamic driving force, ΔG_∞, employed and the correct driving force of critical cluster formation and growth, ΔG_V, which is determined by the real physical state of the critical and near-critical clusters. Since the identity of the driving force of critical cluster formation with the respective macroscopic

values is the only assumption employed in the analysis it has to be removed in order to solve the discussed in this and earlier sections discrepancies. Then we have to admit that the bulk properties of critical and near-critical clusters do not coincide with the properties of the respective macroscopic phases and are not determined correctly employing Gibbs' classical thermodynamic approach. As a direct consequence from this assumption, it follows that both surface energy and thermodynamic driving force must be considered as unknown quantities.

Let us analyze now the above mentioned results introducing a coefficient $K(r)$ that connects the (supposed) real thermodynamic driving force, ΔG_V, with the respective value for the macro-phase, ΔG_∞, as

$$\Delta G_V = K(r)\Delta G_\infty. \tag{43}$$

The coefficient $K(r)$ reflects the fact that the thermodynamic driving force for critical nuclei may differ from that of the corresponding macro-phase. If one denotes by σ^r_{cm} the true value of the surface energy estimated with account of Eq. (43) and takes into consideration that $U \sim \Delta G_V$, the following equations connecting σ^r_{cm} with σ_{cm} and σ^{**}_{cm} are obtained from Eqs. (41) and (42)

$$\sigma^r_{cm} = K(r)^2\sigma_{cm}, \quad \sigma^r_{cm} = K(r)^{2/3}\sigma^{**}_{cm}. \tag{44}$$

Eq. (44) yield

$$K = \left(\frac{\sigma^{**}_{cm}}{\sigma_{cm}}\right)^{2/3}. \tag{45}$$

Thus, both methods provide the same value of crystal/melt surface energy if the reduced thermodynamic driving force, $\Delta G_V = K(r)\Delta G_\infty$, is employed. The values of K presented in Table 2 show a considerable reduction of the thermodynamic driving force for nucleation and growth of critical and near-critical nuclei as compared with that for the macro-crystal growth ($K < 1$). Employing this self-consistently determined value of the driving force, different estimates for the specific surface energy are obtained as compared with the case when the classical Gibbs' approach for the determination of the driving force is used. It should be emphasized that the value of σ^r_{cm} (see Table 2) is smaller than that of σ^*_{cm} and σ^{**}_{cm}. Hence, in this way, the decrease of the thermodynamic driving force results in values of the interfacial energy that are significantly more reasonable (taking Stefan's rule into account). We can conclude, consequently, that the discussed so far grave problems in the theoretical interpretation of crystallization can be removed if one assumes that the state of critical and near-critical clusters is different from the state of the newly evolving macro-phase. That is the classical Gibbs' approach does not give, consequently, in general a correct description of the bulk properties of critical and near-critical clusters.

Arriving at such conclusion, two classes of problems arise: First, one has to discuss whether there exist alternative theoretical concepts favoring this point of view or not and whether it is possible to generalize eventually Gibbs' approach in order to remove mentioned defect in Gibbs' classical treatment. Second, one has to search for the physical origin of such differences in the state of the critical clusters as compared with the respective bulk phases and for additional arguments and experimental results confirming such point of view. Such analysis will be performed in the subsequent sections.

5.4. Bulk properties of critical clusters and properties of the newly evolving macroscopic phase: some results of theoretical analyses

5.4.1. Gibbs' theory of heterogeneous systems: basic postulates, advantages and shortcomings

In the theoretical interpretation of experimental results on the dynamics of first-order phase transitions starting from metastable initial states, up to now the classical nucleation theory has been predominantly employed treating the respective process in terms of cluster formation and growth and employing Gibbs' theory of capillarity. This preference is due to the advantage of Gibbs' approach to the description of thermodynamically heterogeneous systems allowing one to determine the parameters of the critical clusters and the work of critical cluster formation in the nucleation rate expression in a relatively simple way which is based on the knowledge of macroscopic bulk and surface properties of the ambient and newly evolving phases.

In his classical analysis [4], Gibbs describes heterogeneous systems (in application to the problems under consideration, we discuss a cluster of a newly evolving phase in the ambient phase) via an idealized model system. In this model, the real system is described as consisting of two homogeneous phases divided by a mathematically sharp interface. The thermodynamic characteristics of the system are represented as the sum of the contributions of both homogeneous phases and correction terms, the so-called superficial quantities, which are assigned to the interface. They reflect the diffuseness of the interface in the framework of Gibbs' model approach. In contrast to alternative statements [77,78] we believe that such approach is theoretically well-founded and correct provided one is able to determine the superficial quantities in an appropriate way for any real system.

In order to further develop the theoretical concept attempting to solve this task, Gibbs formulated a fundamental equation for the superficial (or interfacial) thermodynamic parameters (specified by the subscript σ) which is widely similar to the fundamental equation for homogeneous bulk phases. For spherical interfaces we restrict our considerations to, it reads [4]

$$\mathrm{d}U_\sigma = T_\sigma \mathrm{d}S_\sigma + \sum \mu_{i\sigma}\mathrm{d}n_{i\sigma} + \sigma\,\mathrm{d}A + C\,\mathrm{d}c, \tag{46}$$

where U is the internal energy, S the entropy, T the temperature, μ_i the chemical potential, n_i the number of particles or moles of the different components ($i = 1,2,\ldots,k$), σ the surface or interfacial tension, A the surface area, and

$c = (1/R)$ the curvature of the considered surface element, while C is a thermodynamic parameter determining the magnitude of changes of the internal energy with variations of the curvature of the considered surface element. R is the radius of curvature of the considered surface element.

An integration of this equation results in

$$U_\sigma = T_\sigma S_\sigma + \sum \mu_{i\sigma} n_{i\sigma} + \sigma A. \tag{47}$$

A combination of both equations yield the Gibbs adsorption equation in the general form

$$S_\sigma \, \mathrm{d}T_\sigma + \sum n_{i\sigma} \, \mathrm{d}\mu_{i\sigma} + A \, \mathrm{d}\sigma = C \, \mathrm{d}c. \tag{48}$$

In order to assign well-defined values to the superficial quantities and cluster size, as an essential requirement of Gibbs' theory the location of the dividing surface has to be specified. In application to nucleation processes, usually the surface of tension is employed. It is defined, utilizing Gibbs' fundamental equation for the superficial quantities, via the equation $C = 0$. For this particular dividing surface, the surface tension does not depend explicitly on the curvature. Moreover, it follows that in the classical Gibbs' approach the surface tension depends on $(k + 1)$ independent state variables.

With Eq. (47) and the well-known expressions for the internal energy of homogeneous bulk phases, we get the following expression for the internal energy of the whole system (e.g., [79–81])

$$U = T_\alpha S_\alpha - p_\alpha V_\alpha + \sum \mu_{i\alpha} n_{i\alpha} + T_\beta S_\beta - p_\beta V_\beta + \sum \mu_{i\beta} n_{i\beta} + T_\sigma S_\sigma + \sum \mu_{i\sigma} n_{i\sigma} + \sigma A. \tag{49}$$

Here p is the pressure, V the volume, the subscript α specifies the parameters of the cluster phase, the subscript β refers to the parameters of the ambient phase.

In application to nucleation, the state of the ambient phase is known. In this way, in order to employ Gibbs' theory, the bulk state of the cluster phase has to be specified. This procedure is performed in Gibbs' classical treatment for *equilibrium states of heterogeneous substances*, exclusively (the title of his paper, Ref. [4], is 'On the equilibrium of heterogeneous substances'), a cluster of critical size in the ambient phase being a particular realization of a thermodynamic equilibrium state. By employing the general conditions for thermodynamic equilibrium [4], two of the three basic sets of the equilibrium conditions are obtained

$$T_\alpha = T_\beta = T_\sigma, \quad \mu_{i\alpha} = \mu_{i\beta} = \mu_{i\sigma}, \quad i = 1, 2, \ldots, k, \tag{50}$$

allowing one to uniquely determine the state parameters of the cluster phase from the knowledge of the state of the ambient phase.

The bulk properties of the critical clusters of the newly evolving phase are determined, consequently, in Gibbs' approach uniquely via the equilibrium conditions Eq. (50) for temperature and chemical potentials of the different components in the two coexisting bulk phases. Hereby the question is not posed whether or not these state parameters represent a correct description of the bulk state parameters of the cluster. It is commonly believed that this is the case. However, Gibbs himself made a comment that, in general, the properties of the critical clusters may differ from the predictions obtained in his approach. It follows further from the Gibbs method that, for the critical clusters, the interfacial tension referred to the surface of tension is uniquely determined by the state parameters of either the ambient or the cluster phase (cf. Eqs. (48) and (50)). Consequently, once the parameters of the ambient phase are given, the surface tension does not depend – according to Gibbs' classical method – on the state parameters of the cluster phase. Moreover, the superficial temperature and chemical potentials are determined by the respective parameters of the bulk phases as well.

As it turns out [80–82], Gibbs' method leads to state parameters of the critical cluster's bulk phase which are widely identical, at least, in application to phase formation in condensed phases, to the properties of the newly evolving macroscopic phases. Modifications of these properties, due to differences in the pressure of small clusters as compared with the equilibrium coexistence of both phases at planar interfaces, as given by the Young–Laplace equation (the third equilibrium condition),

$$p_\alpha - p_\beta = \frac{2\sigma}{r_*} \tag{51}$$

is commonly of minor importance here although the pressure differences may be large. With the numerical estimates $p_\beta = p_{\mathrm{at}} \sim 10^5\ \mathrm{N/m^2}$, $\sigma \sim 0.1\ \mathrm{J/m^2}$, $r_* \sim 10^{-9}\ \mathrm{m}$ (at high under-cooling), we get $\Delta p \sim 2 \times 10^8\ \mathrm{Pa}$ or $2000 p_{\mathrm{at}}$. However, the effect of pressure on the density is small due to the low compressibility of the cluster bulk phase. This result – the wide similarity of the properties of the critical cluster with the properties of the evolving macroscopic phases – is an essential general feature of Gibbs' classical theory not only in application to crystallization. It leads – as discussed in detail here above – to contradictions in the interpretation of experimental results and as we will see below to contradictions with the results of computer simulations and density functional computations of the properties of critical clusters showing a quite different behavior, in particular, for higher supersaturations. So, why Gibbs' theory can be applied at all to nucleation? The following answer can be given.

In application to nucleation, not the knowledge of the properties of the critical clusters is commonly of major interest but instead the value of the work of critical cluster formation, W_*. This quantity is determined in Gibbs' description generally via $W_* \propto \sigma^3/(p_\alpha - p_\beta)^2$ [4] or in a frequently good approximation via $W_* \propto \sigma^3/(\Delta G_V)^2$ (cf. Eq. (4)). For any state of the ambient phase, the driving force of critical cluster formation, which can be considered to be proportional to either $(p_\alpha - p_\beta)$ or ΔG_V, is determined uniquely via the equilibrium conditions Eq. (50). In this way, as far as the process proceeds via nucleation with a well-defined value of the work of critical cluster formation, one can always find a value of the interfacial tension

leading to the correct result for W_*. Such possibility exists independently on whether the driving force is determined in an appropriate way corresponding to the real situation. In general, the interfacial tension (or the specific interfacial energy in application to formation of crystalline critical nuclei) is different from its macroscopic value. This deviation from the macroscopic value is connected then with the idea of a curvature (or supersaturation) dependence of the surface tension. But in such approach, σ looses its meaning of a physical quantity. As we previously mentioned it becomes a fit parameter that compensates the inappropriate choice of the bulk reference states for the description of the critical clusters.

The failure of Gibbs' classical approach for the determination of the bulk properties of the critical clusters is connected with another disadvantage that has seldom been noticed. This classical approach is in deep conflict with the conventional method of determination of saddle points or extremums of hyper-surfaces of any dimension. In order to find these singular points of such surfaces, following the standard methods, one has to first formulate the respective equations for any arbitrary state of the system and then to apply the extremum conditions. In application to cluster formation, we would have first to formulate the thermodynamic potentials for any well-defined thermodynamic (including non-equilibrium) states of a cluster or ensembles of clusters in the ambient phase and then to search for saddle points. This is the general procedure, which is also employed in any density functional computations of the work of critical cluster formation (see the subsequent discussion).

However, Gibbs never tried in his fundamental paper [4] even to formulate the problem of the determination of the thermodynamic potential of a cluster or ensembles of clusters of non-critical sizes in the otherwise homogeneous ambient phase. His method is, consequently, in conflict with the standard theoretical procedure. It follows as another consequence that Gibbs' original treatment cannot supply one with a recipe to determine the state of sub- and supercritical clusters in a well-founded theoretical way. Any description of cluster growth processes, which is based on Gibbs' theory, involves additional assumptions, which may or may not be appropriate. Consequently, a problem arises whether it is possible to develop a generalisation of Gibbs' thermodynamic treatment allowing one to describe critical cluster formation in a theoretically more founded way and supplying one simultaneously with a regular method of theoretical determination of the properties of sub- and supercritical clusters. However, before developing the respective generalization, we briefly summarize some alternative methods of theoretical description and their results concerning the problems under consideration.

5.4.2. Continuum's approaches to the determination of the properties of heterogeneous systems: van der Waals' and modern density functional approaches

About two decades after the formulation of Gibbs' theory, van der Waals [83,84] developed an alternative continuum's approach to the description of heterogeneous systems. In this approach, the interface is characterized by a continuous change of the intensive thermodynamic state parameters from the respective values in one to those characterizing the other of the coexisting phases. The van der Waals method of description of heterogeneous systems was reinvented about 60 years later by Cahn and Hilliard [85] and applied for the description of the properties of critical clusters in nucleation and for the development of the basic ideas of the classical theory of spinodal decomposition.

In the van der Waals and Cahn–Hilliard approach, the Gibbs free energy of a heterogeneous system is given in the simplest version as

$$G(p,T,x) = \int \left[g(p,T,x(\vec{r})) + \kappa(\nabla x(\vec{r}))^2 \right] \mathrm{d}V. \tag{52}$$

For any given concentration profile, the value of the Gibbs free energy can then be found by integrating the volume density, g, of the Gibbs free energy supplemented by the surface term, $\kappa(\nabla x(\vec{r}))^2$, over the whole volume, V, of the system, i.e., any well-defined function, $x(r)$, results in some definite value of the Gibbs free energy. Critical clusters refer to saddle points of the thermodynamic potentials. Consequently, in order to determine the change of the Gibbs free energy in critical cluster formation, one has to search for such concentration or density profiles, for which the respective conditions for a saddle point of the thermodynamic potential G are fulfilled. From a mathematical point of view, the thermodynamic potential is determined, consequently, as a functional of the density or concentration profile giving the name to the method of computation of the work of critical cluster formation (density functional methods; i.e., saddle points are determined via the search for an extremum of the respective functional).

In application to nucleation-growth processes (phase transformations originating from metastable initial states), Cahn and Hilliard came to the conclusion that the bulk state parameters of the critical clusters may deviate considerably from the respective values of the evolving macrophases and, consequently, from the predictions of Gibbs' theory. These results of the van der Waals and Cahn–Hilliard-approach were reconfirmed later-on by more advanced density functional computations (cf., e.g., Refs. [86–88]) allowing one to determine the thermodynamic potential by choosing some well-defined interaction potentials between the particles of the system under consideration. Similarly to the van der Waals and Cahn–Hilliard approach, the spatial distribution of the order parameter field is computed and it is assumed that the different phases and their states can be described by varying the value of the order parameters.

As an example, the composition of a critical cluster in phase formation in a binary solution is shown in Fig. 16 [80]. The supersaturation is changed by varying the molar fraction, x, of one of the components in the ambient phase inside the range from the binodal to the spinodal curves,

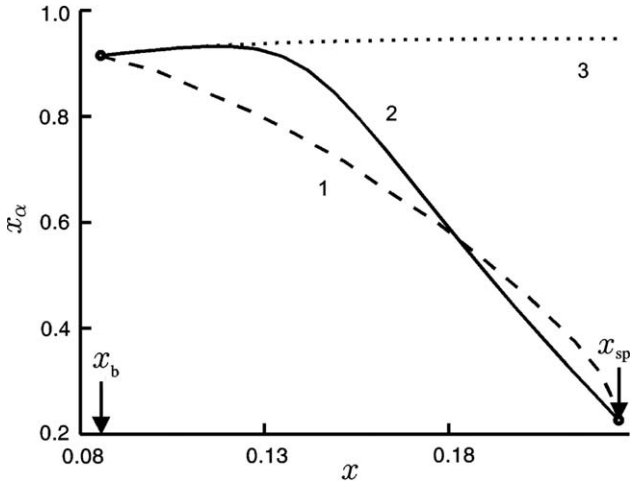

Fig. 16. Composition of the critical cluster, x_α, as a function of the supersaturation for segregation processes in solutions [80]. The molar fraction, x, of the segregating component in the ambient solution can be considered as a measure of supersaturation, which varies in the range between the binodal (x_b) and spinodal (x_{sp}) curves. The dotted curve (curve 3) refers to results of computations of the critical cluster parameters obtained via Gibbs' classical method; the dashed curve (curve 1) to the newly developed generalized Gibbs approach and the full curve (curve 2) to results of density functional calculations of the density in the center of the critical cluster obtained via the van der Waals square gradient method.

i.e., for metastable initial states of the ambient phase. The results of the classical Gibbs approach to the determination of the properties of the critical clusters are given by a dotted curve (curve 3). It is evident that the composition of the critical clusters – determined in such a way – practically does not depend on supersaturation and is widely equal to the value in the newly evolving macroscopic phase. The full curve (curve 2) shows the results for the cluster composition in the center of the critical cluster as obtained via the van der Waals and Cahn–Hilliard square gradient approximation as described by Eq. (52). It is evident that both approaches lead, in general, to very different results. Qualitatively similar results are obtained when the van der Waals and Cahn–Hilliard approach or more advanced density functional computations are applied to the description of crystallization [77,89,90], i.e., the state of the critical cluster differs, in general, from the state of the newly evolving macroscopic phase.

Both Gibbs' and the van der Waals or more advanced density functional methods of description of thermodynamically heterogeneous systems are considered commonly as well-established theories. Nevertheless, only one of them (if any) can be correct in the prediction of the properties of the critical clusters. Moreover, the Gibbs and van der Waals approaches lead to contradicting each other results in the description of the behavior of phase separating systems in the vicinity of the classical spinodal curve (cf. Ref. [91]). In this way, one is confronted here with internal contradictions in two well-established theories, which must be, hopefully, resolved.

The question which of both mentioned theories describes more correctly the properties of the critical clusters can be answered from a theoretical point of view based on the analysis of the results of computer simulation methods of phase formation processes in model systems [92–96]. The respective analyses show that critical clusters do have properties, in general, significantly different from the properties of the newly evolving macroscopic phases (although in some particular cases also results are obtained which are in agreement with the classical Gibbs approach). In this way, computer simulation methods support, in general, the van der Waals or alternative density functional approaches for the description of heterogeneous systems.

Consequently, we can conclude that the majority of existing theoretical approaches for the determination of the work of critical cluster formation gives strong support to the point of view that the state of the critical clusters may significantly differ from the state of the newly evolving macroscopic phases. Consequently, in order to obtain correct expressions for the work of critical cluster formation in the interpretation of experimental results one has to account for a cluster size dependence not only of the surface properties of the critical clusters but also of their bulk properties.

5.4.3. A generalization of Gibbs' classical theory

Having reached such conclusion, immediately the question arises whether it is necessary to abandon the classical Gibbs approach at all or whether it is possible to modify it in such a way that it retains its advantages (use of macroscopic properties of the phases of interest for a determination of the work of critical cluster formation) but overcomes its shortcomings (incorrect determination of the bulk properties of the critical clusters) discussed above. As it turns out such generalization of Gibbs' thermodynamic theory can be really performed. It was initiated several years ago based initially on a generalization of Ostwald's rule of stages in application to nucleation. This generalization of Ostwald's rule was formulated as follows [97]: 'Those classes of critical clusters determine the process of the transformation, which correspond to a minimum work of critical cluster formation (as compared with all other possible alternative structures and compositions, which may be formed at the given thermodynamic constraints)'. This concept was then employed in order to develop a new approach for the determination of the work of critical cluster formation and the determination of critical cluster properties based on a generalization of Gibbs' classical approach [79,98].

In such a generalization of Gibbs' theory, we followed again Gibbs' method of dividing surfaces but started with the analysis of the question how to formulate a thermodynamic description of heterogeneous systems (clusters or ensembles of clusters in the otherwise homogeneous ambient phase) for well-defined non-equilibrium states, when both the clusters and the ambient phase are in an internal thermodynamic equilibrium but the system as a whole is not. Having a look at Eq. (49), immediately the question arises then, how to determine the values of the superficial temperature and chemical potentials for any well-defined non-equilibrium states of the heterogeneous systems under

consideration. Since these parameters cannot be determined independently of the parameters of the coexisting bulk phases, we postulated long ago [99] that generally the conditions

$$T_\beta = T_\sigma, \quad \mu_{i\beta} = \mu_{i\sigma}, \ \ i = 1, 2, \ldots, k, \tag{53}$$

must hold. In other words, it is assumed that the superficial temperature and chemical potentials are determined widely by the properties of the ambient phase (with known properties). *Note that the bulk state parameters of the cluster phase may vary independently and may have so far arbitrary values*. Employing such condition and the fundamental equation for the superficial quantities Eq. (46) as formulated by Gibbs, the interfacial tension (referred to the surface of tension) becomes then a function of the state parameters of the ambient phase exclusively. However, for non-equilibrium states the interfacial tension has to depend, in general, not only on the properties of the ambient but also on all intensive state parameters of the cluster phase. This set of intensive state parameters of the cluster phase we denote here as $\{\varphi_{i\alpha}\}$. In order to be able to describe such additional dependence, Gibbs' fundamental equation Eq. (46) has to be generalized resulting in (see also [79,82] for further details)

$$\mathrm{d}U_\sigma = T_\sigma \,\mathrm{d}S_\sigma + \sum \mu_{i\sigma}\,\mathrm{d}n_{i\sigma} + \sigma\,\mathrm{d}A + C\,\mathrm{d}c + \sum \phi_{i\alpha}\,\mathrm{d}\varphi_{i\alpha}, \tag{54}$$

where $\phi_{i\alpha}$ are parameters determining the magnitude of variations of the superficial internal energy with respect to variations of the bulk state of the cluster phase.

Since all parameters $\varphi_{i\alpha}$ of the cluster phase, entering Eq. (54), are intensive quantities, the expression for the superficial internal energy Eq. (47) and also for the thermodynamic potentials are formally not changed as compared with Gibbs' original approach. In contrast, the generalized Gibbs' adsorption equation reads now

$$S_\sigma\,\mathrm{d}T_\beta + \sum n_{i\sigma}\,\mathrm{d}\mu_{i\beta} + A\,\mathrm{d}\sigma = C\,\mathrm{d}c + \sum \phi_{i\alpha}\,\mathrm{d}\varphi_{i\alpha}. \tag{55}$$

In the generalization of Gibbs' approach, the interfacial tension can and must be considered consequently as a function both of the intensive state variables of the ambient and the cluster phases and curvature. For the surface of tension (defined also in the generalized Gibbs approach via $C = 0$) an explicit curvature dependence of the surface tension does not occur, again.

Having at ones disposal the thermodynamic potentials for the respective non-equilibrium states, the equilibrium conditions are obtained by known procedures employed already by Gibbs in his classical model approach [4]. They differ from the equilibrium conditions derived by Gibbs and read, in general,

$$r_* = 2\sigma \Big/ \Big[p_\alpha - p_\beta - \sum \rho_{i\alpha}(\mu_{i\alpha} - \mu_{i\beta}) - s_\alpha(T_\alpha - T_\beta)\Big], \tag{56}$$

$$\mu_{i\alpha} - \mu_{i\beta} = (3/r_*)(\partial\sigma/\partial\rho_{i\alpha}), \tag{57}$$

$$T_\alpha - T_\beta = (3/r_*)(\partial\sigma/\partial s_\alpha). \tag{58}$$

Here p is the pressure, ρ the volume density of the ($i = 1, 2, \ldots, k$) different components in the system, s is the volume density of the entropy. The subscript α specifies, again, the parameters of the cluster, while β refers to the parameters of the ambient phase.

In order to determine the parameters of the critical clusters, one has to know the values of the surface tension (or the specific interfacial energy). In the simplest case [79,82,98,100], it can be expressed as a quadratic form in the differences of the state parameters of the ambient ($\{\varphi_{i\beta}\}$) and cluster ($\{\varphi_{i\alpha}\}$) phases as

$$\sigma = \sum\sum \Xi_{ij}(\varphi_{i\alpha} - \varphi_{i\beta})(\varphi_{j\alpha} - \varphi_{j\beta}). \tag{59}$$

The values of the parameters Ξ_{ij} can be determined then from the knowledge of the specific interfacial energy for phase coexistence at planar interfaces.

As it turns out, the work of critical cluster formation can be written generally again in the well-known classical form

$$W_* = \tfrac{1}{3}\sigma A_*, \tag{60}$$

where A_* is the surface area of the critical cluster. Note however that the results for the numerical values for the work of critical cluster formation are different in both discussed classical and generalized Gibbs' approaches since the state parameters of the clusters differ in these two methods.

In general, the parameters of the critical clusters as obtained via the generalized Gibbs approach differ significantly from the parameters obtained following the classical Gibbs method. However, for phase equilibrium of macroscopic systems, the equilibrium conditions derived in the generalized Gibbs approach coincide with Gibbs' classical expressions (here the radius of the critical clusters tends to infinity and the classical Gibbs equilibrium conditions are obtained as a special case). Note that Gibbs' classical equilibrium conditions are retained in the above given generalized equations also as a limiting case when the derivatives of the interfacial specific energy with respect to the intensive state parameters of the cluster phase are set equal to zero.

Employing the generalized Gibbs' approach to the determination of critical cluster properties for a variety of phase-separating systems (segregation in solutions [80], condensation and boiling in one-component fluids [81], boiling in multi-component fluids [82]) it has been shown that the predictions concerning the properties of critical clusters and the work of critical cluster formation, derived in the generalized Gibbs' approach, are in agreement with van der Waals' and more advanced density functional methods of determination retaining, on the other hand, the simplicity in applications similarly to the classical Gibbs method as an additional advantage. For example, in Fig. 16 the composition of the critical clusters as obtained via the generalized Gibbs approach is shown by a dashed curve (curve 1). For small supersaturations, the results of all mentioned approaches agree, however, when

the whole range of initial supersaturations is considered and especially for large supersaturations the results of the generalized Gibbs' approach are similar to the results obtained via square gradient density functional computations and deviate significantly from the results of Gibbs' classical approach. Such kind of behavior is essential in order to guarantee the vanishing of the surface free energy and of the work of critical cluster formation near the classical spinodal curve, two features commonly considered as essential for a correct description of nucleation and which are not described by the classical approach when the capillarity approximation is utilized [88]. It can be shown further in a general way [99] that the classical Gibbs approach employing in addition the capillarity approximation as a rule overestimates the work of critical cluster formation and, in general, significantly.

Recently the generalized Gibbs' approach was further extended [91,101–104] to allow the description not only of nucleation but also of growth and dissolution processes taking into account changes of the bulk and surface state parameters of the clusters as a function of supersaturation and size. Hereby a criterion was advanced to allow one the quantitative determination of the changes in the bulk and surface properties of the clusters in the course of their growth. As a first application, this new theory of growth and dissolution processes was applied to the analysis of segregation in solutions. However, the method is generally applicable. In the framework of this approach, the change of a variety of thermodynamic and kinetic properties with cluster size has been determined for the first time such as the change of the surface tension, the driving force of cluster growth, the dependence of the effective diffusion coefficients on cluster size, etc. As it turns out the respective thermodynamic and kinetic parameters may change significantly in dependence on cluster size. In this way, the estimates of these parameters obtained from nucleation data may not be appropriate for the description of growth processes of clusters of macroscopic sizes and vice versa. This result gives a new key to the solution of the problems posed by Granasy and James [105] that growth rates computed with values of kinetic coefficients obtained from nucleation data may lead to deviations between theory and experiment reaching several orders of magnitude. Even peculiarities in the evolution of the cluster size distributions – like the development of bimodal distributions in intermediate states of the nucleation-growth process and unexpected properties – may be explained straightforwardly based on these concepts [102,104,106,107]. Thus, in a correct theoretical treatment not only deviations of the composition of the critical nuclei from those of the respective macroscopic phases, but also variations in the composition of the sub- and supercritical crystals have to be and can be accounted for.

The extension of these concepts in application to crystallization is in progress. Here, in addition to changes in composition and density also possible differences in the structure of the critical clusters (and their mutual interdependence with concentration fluctuations [12,88,108,109]), as compared with the state of the crystalline macro-phase, and its possible change in the course of the growth of the supercritical crystallites have to be taken into consideration (cf., e.g., [110–112]).

5.4.4. Discussion

Let us first briefly summarize the results of the preceding subsection: In order to develop a consistent theoretical method of determination of the properties of the critical clusters, we have generalized Gibbs' theory starting with the thermodynamic description of non-equilibrium states and including in this way into the theoretical schema the possibility of description of clusters of sub- and supercritical sizes in the ambient phase. In order to realize such task, Gibbs' fundamental equation for the superficial thermodynamic state parameters was generalized to allow one, in particular, an incorporation into the theory of the dependence of the interfacial or surface tension both on the state parameters of the ambient and the newly evolving cluster phases, respectively. Such essential additional step in the generalization of Gibbs' classical approach was not done in earlier own work [99] and also not in the two (to the knowledge of the authors) existing alternative generalizations of Gibbs' theory to non-equilibrium states (see [113]). By this reason, in latter mentioned approaches [99,113] the equilibrium conditions retain the same form as in the classical Gibbs' approach.

Following the generalized Gibbs' approach, it is possible to determine the properties of the critical clusters in a new way. We arrive at relations, which are, in general, different as compared with the predictions of the classical Gibbs approach. The respective results are – for model systems – in agreement with density functional computations and results of computer simulations. Moreover, since we have formulated a consistent description of clusters in thermodynamically non-equilibrium states, regular methods can be and are developed to determine also the properties of clusters of sub- and supercritical sizes in dependence on supersaturation and their sizes. In this way, a new tool for the description of nucleation-growth processes, in general, and crystallization processes in glass-forming liquids, in particular, has been developed allowing one to interpret a variety of experimental findings from a new point of view [91,102–104,111].

As an alternative non-classical method of theoretical treatment of crystallization going back already to van der Waals [83,84], the van der Waals and Cahn–Hilliard square gradient density functional approach is employed presently intensively for the interpretation of nucleation in crystallization processes [77,87–89,114]. These studies are supplemented by the analysis of nucleation-growth processes based on so-called phase field models, a dynamic extension of the van der Waals and Cahn–Hilliard approach [78,87,115–118], allowing one the determination of the evolution of the order-parameter fields with time. These types of analyses are confronted, however, with one principal

problem, which has to be taken into consideration – as it seems to us – more carefully in future. This problem is the prediction – in the framework of mentioned van der Waals and Cahn–Hilliard type approaches – of spinodal curves in melt-crystallization.

More then three decades ago, Skripov and Baidakov [119], based on the analysis of experimental and computer simulation data – advanced the conjecture about the non-existence of a spinodal curve in one-component melt crystallization processes (or widely equivalent to them polymorphic transformations where liquid and crystal phases have the same composition). It was emphasized that this statement is in agreement with the point of view of the non-existence of a critical point in liquid–solid phase equilibriums and of a necessarily discontinuous transition between liquid and crystal [120]. A further detailed proof of this statement in a period of about 30 years resulted in a confirmation of its validity [74,121]. An additional support of such point of view can be obtained from the analysis of experimental data on crystallization processes of liquids, in general, and glass-forming melts, in particular. Such analysis does not give any indication on the existence of spinodal curves in crystallization processes of the considered type [12]. The latter conclusion is supported, for example, by Oxtoby [87,88] and Granasy and James [77].

However, density functional theories of crystallization predict in a variety of cases the existence of spinodal curves. Since such kind of behavior is not found by experiments, parameters are chosen that transfer the spinodal into parameter regions, where – due to the high viscosity – phase formation processes cannot occur [77,87,122,123]. A spinodal type behavior is also predicted in some cases by Granasy's so-called diffuse interface theory and even close to the glass transition temperature [124]. Provided – as we believe – the conjecture of Skripov and Baidakov is correct, the prediction of a spinodal in the mentioned theories leads to some serious doubts into their applicability to melt crystallization, at least, in the present form. A theory cannot be correct if it predicts – not as an exception but as a rule – phenomena, which are absolutely not observed in nature. By the above discussed reasons, a further detailed analysis of the basic ideas and limitations of density functional approaches in application to melt crystallization seems to be absolutely essential.

Completing the discussion on the limitations of the classical Gibbs approach to the description of the properties of critical clusters, we would like to add a few comments on the so-called 'nucleation theorem' [125–128] employed frequently in order to determine the properties of critical clusters based on nucleation rate data [88,94,96,129,130]. In an approximate form and for one-component systems, the content of this theorem can be formulated as [125]

$$dW_*/d\Delta\mu \approx -n_*, \tag{61}$$

i.e., derivatives of the work of critical cluster formation (or the steady-state nucleation rate) with respect to the state parameters of the ambient phase allow one to determine the parameters of the critical clusters. Relations of this type – derived in the framework of Gibbs' classical theory and employing the capillarity approximation – have been known for a long time. The increased interest in dependencies of such type resulted from the statements by Kashchiev [125] that the nucleation theorem is valid independent of the method employed for the thermodynamic description and valid for any kind of phase transformation and size of the critical clusters considered. However, the independence of the mentioned relation on the way of description of the clusters is questionable already on general argumentations. For example, Einstein noted in a conversation with Heisenberg on the foundations of quantum mechanics that *it is the theory which determines what can be measured*. In a detailed analysis of the results of Ref. [125] it has been shown recently in detail [127,128] that all above mentioned statements concerning Eq. (61) are not correct.

In an extension of the analysis of Ref. [125], Oxtoby and Kashchiev developed similar relations in application to multi-component systems [126]. In this analysis, Gibbs' classical theory of thermodynamically heterogeneous systems was employed without introducing any additional assumptions like the capillarity approximation, i.e., the assumption that the surface tension of critical clusters is equal to the respective value for an equilibrium coexistence of both phases at planar interfaces. Consequently, the mentioned generalizations of the nucleation theorem are of the same level of validity in application to experiment as the classical Gibbs approach. They can describe the parameters of the real critical clusters correctly only as far as Gibbs' classical method is adequate to the considered particular situation. Having in mind the above discussed limitations of Gibbs' classical approach in the description of the parameters of critical clusters, mentioned generalizations of the nucleation theorem do not supply us, in general, with a description of the real critical clusters but merely with a description of Gibbs' model clusters resulting in the same value of the work of critical cluster formation as for the real critical clusters. Consequently, also the correctly derived – in the framework of the classical Gibbs' approach – versions of the nucleation theorem do not describe, in general, the parameters of the real critical clusters.

Since the generalized Gibbs approach allows one a determination of the parameters of the critical clusters, that is, for model systems, in agreement with density functional computations and computer simulation studies, it is of interest to prove whether dependencies similar to the 'nucleation theorem' can be formulated also in this generalization of the classical Gibbs approach. The respective work is in progress.

Finally, we would like to note that there exist also approaches connecting the deviations of the experimental data on crystallization and growth with the effect of static disorder in the melts [131] or the existence of so-called floppy and rigid modes in glasses [132–134].

5.5. Compositional changes of the crystal nuclei at nucleation-growth process: some experimental findings

The formation of solid solutions is a common phenomenon in silicate systems. By this reason, it is important to keep in mind that the critical nuclei can be a proper solid solution with thermodynamic properties, which may differ considerably from those of the finally evolving macroscopic phase. Thus, we can expect that contradictions between experimental results and theoretical predictions concerning nucleation rates and growth kinetics in such systems would be considerably diminished even neglecting for some time possible deviations in the critical nuclei structure as compared with the evolving macro-phase.

The following reasons could generally lead to a difference in the bulk properties of the critical and near-critical crystallites as compared with the respective newly evolving macroscopic phase and to a reduction of the thermodynamic driving force: (a) It is reasonable to assume that near-critical nuclei are less ordered than the material in the corresponding bulk phase and it is possible to show that, in this case, $\Delta G_V < \Delta G_\infty$ holds [69]. (b) According to the model of ideal associated solutions [135,136], a glass-forming melt can be considered as a solution of oxide components and salt-like (stoichiometric) phases. Then, critical cluster formation could be represented as a segregation process in a multi-component solution. As shown in Ref. [97], in this case, the driving force may be smaller than for the macroscopic phase. (c) The deviation of the critical nuclei composition from that of the evolving macro-phase (e.g., owing to the formation of metastable phases or solid solutions) has also to reduce the thermodynamic driving force, as compared with that for the stable macro-phase. This effect, i.e., the deviation of the critical nuclei composition from those of the evolving macro-phase and the parent *stoichiometric* glass was recently observed [137] and is discussed in detail below.

Within certain limits, addition, removal or replacement of different components can continuously change the composition of a given crystallographic system. Hence, generally speaking, compositional variations of critical nuclei of a new phase and, consequently, variations of their properties as compared with those of the corresponding macro-phase could be expected. Indeed such deviations were observed in both stoichiometric $Na_2O{\cdot}2CaO{\cdot}3SiO_2$ glass and glasses belonging to the solid solution (s/s) region between $Na_2O{\cdot}2CaO{\cdot}3SiO_2$ ($N_1C_2S_3$) and $Na_2O{\cdot}CaO{\cdot}2SiO_2$ ($N_1C_1S_2$) [137]. Ref. [137] shows that the formation of stoichiometric crystals occurs via nucleation of s/s whose composition continuously approaches the stoichiometric one and arrives at that in the final stage of crystallization. Figs. 17 and 18 show the evolution of crystal and glassy matrix compositions and the corresponding change of the lattice parameter, respectively. An extrapolation of the change of crystal composition to zero time (or zero volume fraction, $\alpha = 0$, of the crystallized phase) gives a strong indication that the critical clusters are also enriched in sodium.

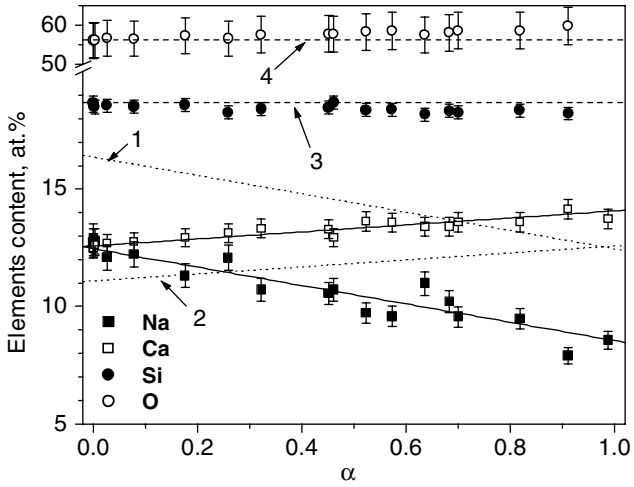

Fig. 17. Composition of the glassy matrix, measured by EDS (points), and of crystals calculated from the parent glass composition, $N_1C_2S_3$, (dotted lines 1 and 2 – Na and Ca, respectively) versus volume fraction crystallized at $T = 650$ °C. Solid lines fit the experimental data. Dashed lines 3 (Si) and 4 (O) refer to the parent glass composition [137].

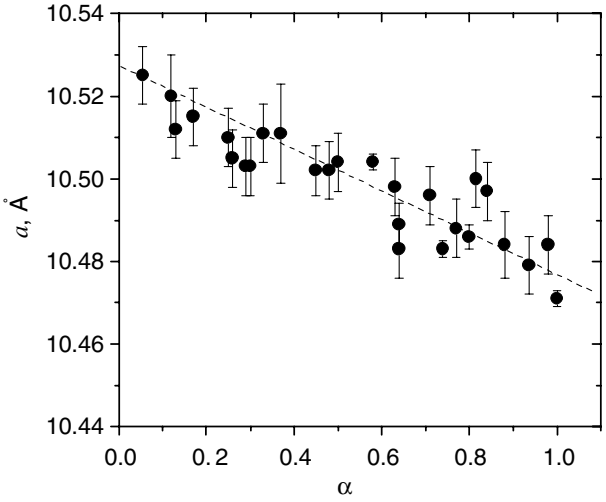

Fig. 18. Lattice parameter of the hexagonal crystal cell of the solid solutions against volume fraction of crystalline phase in stoichiometric $N_1C_2S_3$ glass heat-treated at 650 °C [137].

The exhaustion of sodium in the glassy matrix during crystallization leads to an inhibition of nucleation and crystal growth. According to an analysis of the overall crystallization kinetics using crystal growth data [137], the nucleation process is terminated if about 20% of the volume is crystallized. Fig. 19(a) and (b) shows the volume fraction of crystals and the size of the largest crystals as a function of heat treatment time at $T = 650$ °C for a glass of stoichiometric composition $N_1C_2S_3$. Nucleation takes place up to $t \sim 150$ min ($\ln(t) = 5$): $n \approx 4$, $m \approx 1$, $k = n - 3m \approx 1$ ($n = k + 3m$) (see Eq. (24)). This conclusion is confirmed by a $N(t)$-plot obtained by the 'development' method (see Fig. 19(c)). But, at $\ln(t) > 5$ crystallization proceeds only by crystal growth with $m \approx 0.33$, $n \approx 1$, $k \approx 0$ ($n = 3m$).

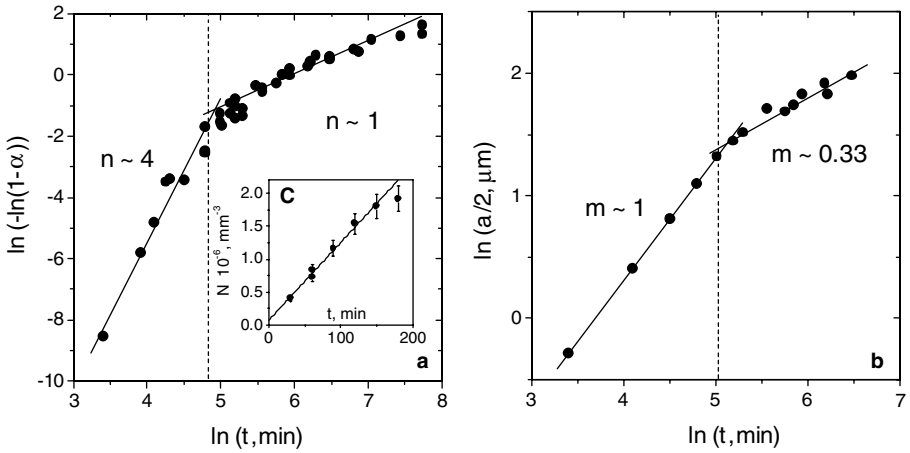

Fig. 19. Volume fraction of crystals (a), size of largest crystals (b), and number of crystals (c) as a function of heat treatment time at $T = 650$ °C for stoichiometric glass $N_1C_2S_3$ [137].

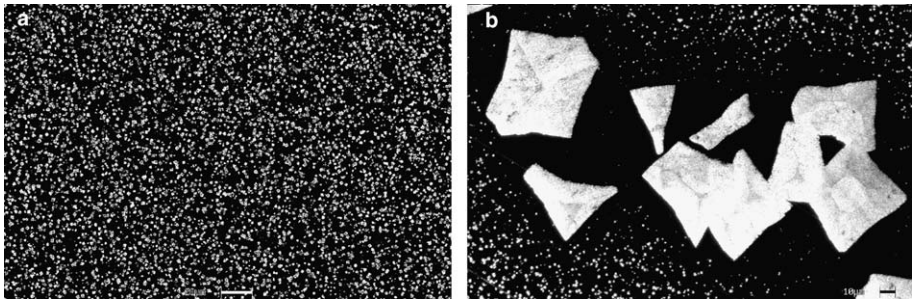

Fig. 20. SEM micrographs of $N_1C_2S_3$ glass subjected to single (a) and double (b) stage heat treatments: (a) $T = 590$ °C, $t = 1560$ min; (b) $T_1 = 720$ °C, $t_1 = 20$ min and $T = 590$ °C, $t = 1560$ min. The bars have a length of (a) 20 μm and (b) 10 μm.

Na-depleted diffusion fields around the growing crystals can be visualized by a second heat treatment at a temperature corresponding to reasonable values of nucleation and growth rates. A comparison of the samples subjected to single-stage (cf. Fig. 20(a)) and double-stage (cf. Fig. 20(b)) heat treatments reveals that pre-existing crystals (formed in first heat treatment) diminish the number of crystals nucleated in the subsequent treatment. Refs. [48,138] show that the nucleation rate decreases with decreasing sodium content in the glass. Hence, it is apparent that the areas observed around the large crystals refer to diffusion fields. A similar transformation path was observed for glasses of compositions between $N_1C_2S_3$ and $N_1C_1S_2$, with the only difference that fully crystallized glasses are s/s with compositions of the parent glasses.

According to the results presented in Fig. 21, the difference between the compositions of the critical nuclei and the parent glass diminishes as the latter approaches the boundary of s/s formation. The deviation of the nuclei composition from stoichiometry (glass $N_1C_2S_3$) or from the initial glass compositions (glasses of the s/s region) diminishes the thermodynamic driving force for crystallization, ΔG_V, and increases the thermodynamic barrier for nucleation. Moreover, this deviation also may lead to an increase of the kinetic barrier. Nevertheless, nucleation of crystals with

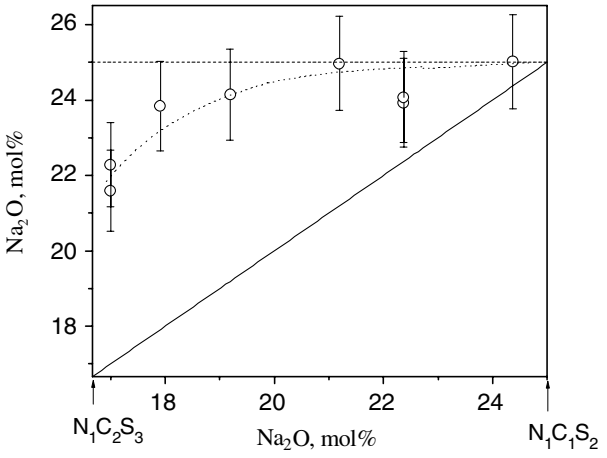

Fig. 21. Sodium oxide content in the critical nuclei versus composition of the parent glass. The solid line represents the case when the compositions of the critical nuclei and the parent glasses are the same.

changed compositions (as compared with those of the parent glasses) actually takes place. Hence, the decrease in ΔG_V must be compensated by a decrease in surface energy in Eq. (4). However, the determination of the variation of the surface energy with composition is not a trivial problem and warrants further study.

Deviations of the composition of the smallest crystals (50 nm) from that of the ambient glass have also been observed for surface crystallization of μ-cordierite in a glass of cordierite composition. But the composition of the largest μ-cordierite crystals (>1 μm) was equal to that of the parent glass [139]. Variations of the crystal compositions during phase transformation were also found in $CaO–Al_2O_3–SiO_2$ glasses [140]. A direct experimental proof of changes of crystal composition with size in crystallization of Ni(P)-particles in hypoeutectic Ni–P amorphous alloys was recently reported in Refs. [106,107].

All mentioned results give a further experimental confirmation of the thesis of a considerable variation of the properties of the clusters in the course of their evolution corroborating the predictions of the generalized Gibbs' approach.

5.6. Independent estimate of the time-lag for nucleation from nucleation and growth kinetics

It was correctly claimed in Ref. [141] that another problem may occur in the treatment of nucleation-growth process in glasses. For a glass with a composition close to lithium disilicate, it was shown in Ref. [141] that the induction time for crystal growth, t_{gr}, estimated (as illustrated by Fig. 22) from a $R \sim t$ plot, where R is the size of the largest crystal experimentally observed, and t the time elapsed from the beginning of the nucleation-growth process, strongly exceeds the induction period for nucleation ($t_{ind} = \frac{6}{\pi^2}\tau$, see Eq. (11)). Latter value was estimated from an $N \sim t$ plot obtained by the 'development' method. However, if crystal nucleation and growth rates refer to the formation of the same phase, t_{gr} and t_{ind} are expected to be similar [21]. In other words, it is reasonable to assume that after an elapsed time t_{gr} the first supercritical nuclei have formed, which then deterministically grow up to sizes visible under an optical microscope.

The discrepancy in induction times reported in Ref. [141] has also been observed for lithium silicate glasses containing 32.6–38.4 mol% Li_2O [142] belonging to the composition range where solid solution crystals precipitate via homogeneous nucleation [143,144]. An example of $N \sim t$ and $R \sim t$ plots for lithium silicate glass with 35.1 mol% Li_2O at $T = 460$ °C is shown in Fig. 22, while Fig. 23 shows the time parameters t_{ind} and t_{gr} estimated at different temperatures for lithium silicate glasses with 33.5 and 32.6 mol% Li_2O. Since the $N \sim t$ curve was obtained by the 'development' method (see Section 3.2), t_{ind} is overestimated as compared with the correct value corresponding to the nucleation temperature. (In Ref. [145] measurements of nucleation and growth rates and corresponding time-lags in lithium disilicate glass were undertaken using *single-stage* heat treatments at a relatively high temperature, 500 °C > T_{max} = 455 °C. The estimated (extrapolated) nucleation time-lag was considerably *higher* than that obtained by the 'development' method. We now think that this result was probably due to insufficient stereological corrections of the crystal number density of the samples subjected to single-stage treatments; see Section 3.4.) Thus, the t_{gr}/t_{ind} ratios experimentally obtained in the cited references are only a lower bound for the difference between the real induction periods. To correct the value of t_{gr} to partly resolve the above discussed problem, an attempt was undertaken in Ref. [141] to account for the effect of a size dependent growth rate. However, the discrepancy between induction times independently estimated from nucleation and growth experiments remained too high. By this reason, it was suggested that initially nucleation of metastable

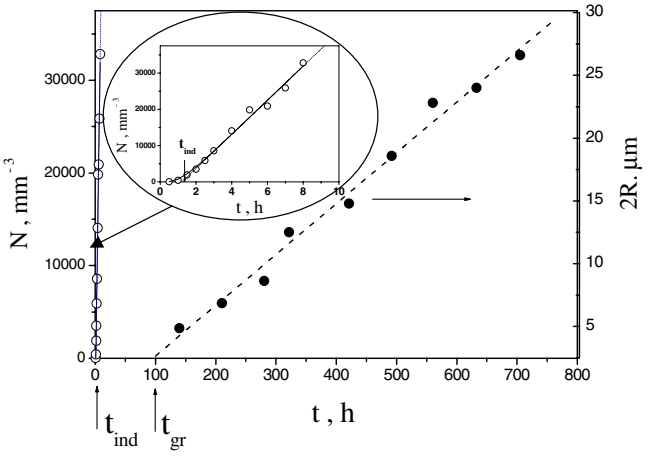

Fig. 22. Number density of crystals, N, and size of the largest crystals, $2R$, versus time of heat treatment at $T = 460$ °C for a lithium silicate glass with 35.1 mol% Li_2O. The inset shows the $N \sim t$ data on a larger scale. The solid line was plotted with Eq. (10) and the dashed line is a linear fit of the $2R(t)$-data [142].

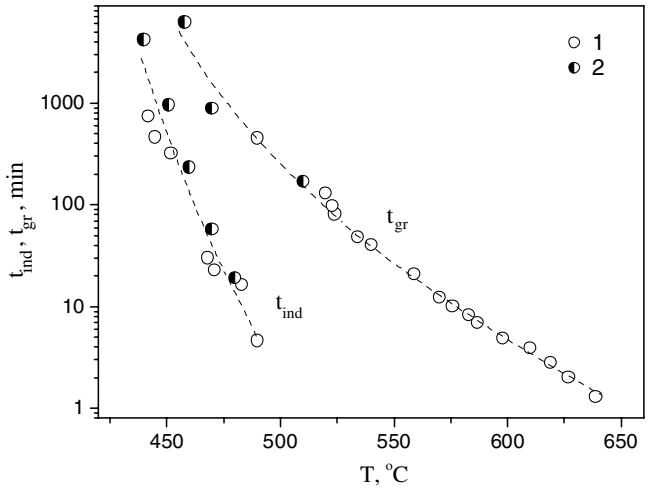

Fig. 23. Induction periods for crystal nucleation, t_{ind}, and for crystal growth, t_{gr}, versus temperature for lithium silicate glasses with 32.6 mol% (points 2) Li_2O [142] and 33.5 mol% (points 1) Li_2O [141]. t_{ind} were taken from N versus t plots obtained by the 'development method' (they are thus overestimated, see text) while t_{gr} were estimated from single-stage experiments at each temperature.

phase crystals take place, which grow more slowly than the macroscopic crystals of the stable phase.

Weinberg [146] questioned the conclusions of Ref. [141] with the argument that the induction time for growth *cannot* be uniquely determined because it depends on the cluster size for which the measurements are performed. He also stated that the induction time for growth becomes unbounded even for measurements performed at large cluster sizes. Strictly speaking those arguments are correct, but since the growth rate *tends* to time-independent values fairly rapidly with increasing R (see, e.g., Eq. (39) or Eq. (62) and Fig. 24), the induction time also tends to a practically finite value when the measurements are extended to large (optical microscopy scale) crystal sizes. Consequently, we believe that the comparison of induction times independently obtained by nucleation and growth experiments can be a useful tool, and, in principle, allows one to draw conclusions similar to those of Ref. [141].

Nevertheless, the results and analysis of induction times for growth deserve some comments. The analysis carried out in Ref. [141] was based on the solution of macroscopic growth equations starting with an initial cluster radius equal to the critical cluster size. With such initial condition, the induction time for growth tends to infinity independently of any particular growth mechanism, since $U(r_*) = 0$, and the numerical integration employed in Ref. [141] could not resolve this problem. In other words, the macroscopic growth equation is not valid for $R = r_*$ and cannot be employed to describe the change of the nuclei size close to the critical one. Recall that according to the Zeldovich–Frenkel equation, in the vicinity of the critical cluster size the 'motion' of the clusters in cluster size space is mainly governed by diffusion-like processes in cluster size space under the action of the concentration gradient with respect to the cluster size distribution function, and thus it is not governed by the thermodynamic driving force, as it is the case in deterministic growth. In addition, the discrepancy observed in Ref. [141] could also be explained in different ways, and not only via the assumption of formation of metastable phases.

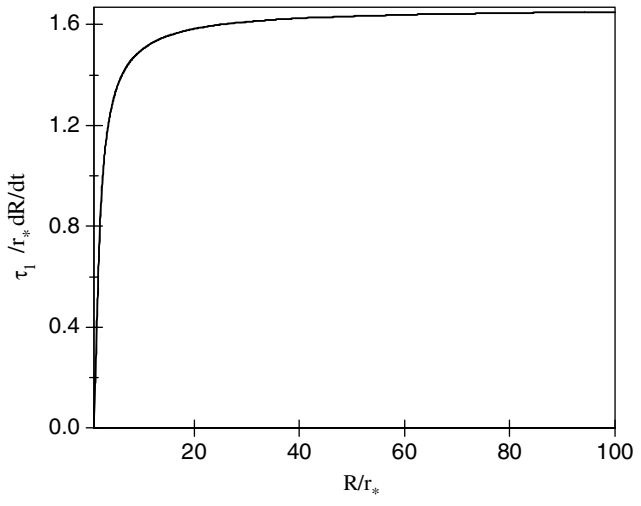

Fig. 24. Crystal growth rate (dR/dt) in (r_*/τ_1)-units versus reduced crystal size according to Eq. (62).

To reconsider the above mentioned problem from a different perspective, we employed an analytical solution of the Fokker–Planck or Frenkel–Zeldovich equation describing nucleation-growth process (cf. Ref. [147]). According to this analysis, for nuclei with sizes larger than two critical sizes, $R > 2r_*$, the following relation holds:

$$\hat{\tau} = \tfrac{3}{5}\left[\widehat{R} + \ln(\widehat{R} - 1) + \tfrac{2}{3}\right]. \tag{62}$$

In Eq. (62) the following dimensionless variables are used:

$$\widehat{R} \equiv \frac{R}{r_*}, \quad \hat{\tau} \equiv \frac{t}{\tau_1}. \tag{63}$$

Here τ_1 is the period of time needed to establish a steady-state cluster size distribution in a range of cluster sizes slightly exceeding the critical size, i.e., it is practically equal to the time required to establish a steady-state nucleation rate for clusters of critical sizes. Recall that, according to Eq. (9) or (10), to practically establish a steady-state nucleation rate a time period about 5τ is required (see Fig. 6(b)). Hence the following relation between τ_1 and τ exists

$$\tau_1 \cong 5\tau. \tag{64}$$

It should be emphasized that Eq. (62) was derived with the following (strong) assumptions commonly employed in CNT:

(i) The bulk state of the clusters is independent on their sizes and is identical to that of the newly evolving macroscopic phase;
(ii) The mechanism of cluster growth does not depend on cluster size, and growth is kinetically limited.

The term 'kinetically limited' refers to the ballistic growth mechanism, where the growth process is only limited by diffusion across the interface, and does not depend on bulk diffusion, as it is the case, for instance, for significant compositional differences between the liquid phase and growing crystal.

The experimental $R(t)$ data were fitted to Eq. (62) using τ_1 and r_* as fit parameters [142]. Fig. 25 shows the result of such calculations. In this way, in order to arrive at the $R(t)$-dependence we did not use any macroscopic growth equation, but relied instead on an analytical solution of the Frenkel–Zeldovich equation, which gives a correct description of the evolution of the cluster ensemble. In addition, in our approach, we do not determine an induction time for growth, but instead determine the time-lag for nucleation by fitting experimental growth data to the nonlinear Eq. (62). Hence, even if Weinberg's comments [146] about the impossibility of defining t_{gr} from $R(t)$ curves are strictly correct, they do not affect our analysis.

The value of τ_1 exceeds the corresponding nucleation induction time, 5τ, estimated from the $N \sim t$ curve, by

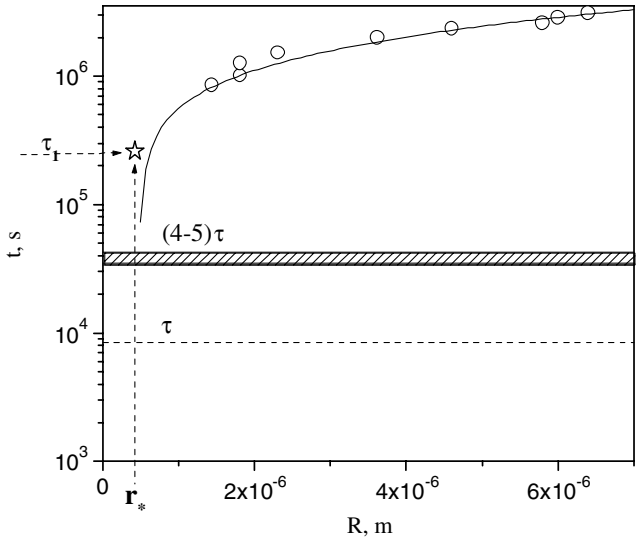

Fig. 25. Time necessary for a crystal to achieve a size R in a lithium silicate glass with 32.6 mol% Li_2O at 460 °C. The full curve was plotted by Eq. (62) using τ_1 and r_* as fit parameters. The coordinates of the open star show the fit parameters τ_1 and r_*. The circles refer to the experimental data. The dashed horizontal line shows the value of the time-lag for nucleation τ estimated by a fit of the $N \sim t$ data to Eq. (10). The crosshatched band corresponds to the time when the nucleation rate achieves 95–99% of its steady-state value [142].

about one order of magnitude (see Fig. 25). However, provided the conditions (i) and (ii) are fulfilled, one expects that τ_1 must be equal to about 5τ, see Eq. (64), since both τ_1 and τ refer to nucleation kinetics. This discrepancy leads to the following conclusion: *at least one or both of the assumptions underlying the derivation of Eq. (62) are not valid.*

In order to explain the present results, one should recall the assumptions made in the derivation of the above equations. In particular, one can assume that the compositions of near-critical clusters deviate from those of the macroscopic crystals to which the crystal size measurements refer. Since in the advanced stages of crystallization the composition of the macro-crystals coincides with those of the ambient melt, this assumption leads to the conclusion that growth of near-critical nuclei is limited by diffusion and is thus not kinetically determined. Moreover, as shown in the analysis of a model system [102], the size dependence of the cluster composition results in a cluster size dependence of a variety of thermodynamic and kinetic parameters (driving force, surface tension, effective diffusion coefficients, and growth rates). These deviations are not taken into account in the derivation of Eq. (62).

Consequently, the mentioned deviations can be interpreted as an additional indication that the classical approach to the description of nucleation-growth processes is insufficient for an interpretation of experimental results on crystallization in lithium disilicate glasses. One of the possible solutions is the assumption of a size (and eventually structure) dependent composition of the crystallites. For completeness we should also to mention an alternative approach [148,149] connecting the possible deviations with possible (cluster-size dependent) solute depletion and volume diffusion in nucleation. Taking into account the results of the generalized Gibbs' approach, density functional studies and computer simulation methods of the properties of critical clusters, the first interpretation of the deviations between the time-lag established in two independent ways (being the result of the change of both cluster properties and growth kinetics in dependence on their sizes) seems to us to be a more convincing explanation.

The questions under which conditions and in what way nuclei change their properties and the growth mechanism are not trivial to answer, especially if these changes occur in the early stages of crystallization. However, the transformation must finally lead to the formation of a stable macrophase with well-defined properties. One of the possible and often assumed ways to account for such effects – the formation of metastable phases – will be discussed in Section 5.7 However, metastable phase formation is not the only possible but a very particular explanation for such kind of behavior (see, e.g., Section 5.5). The analysis of already mentioned model system (segregation in regular solutions [102]) shows that clusters may continuously change their properties with their sizes and do not have the properties of some fictive metastable phase. Such explanation for the observed discrepancy is more general and could be ascribed to the formation of different transient phases more or less continuously changing their properties in dependence on cluster size.

5.7. On the possible role of metastable phases in nucleation

As mentioned in Sections 5.3 and 5.5 the precipitation of metastable phases in the early stages of nucleation may be one of the reasons for the deviation of the critical nuclei properties (e.g., composition) from that of the evolving (stable) macro-phase. The formation of metastable phases is consistent with the original formulation of Ostwald's *Rule of Stages* according to that, 'if the supersaturated state has been spontaneously removed then, instead of a solid phase, which under the given conditions is thermodynamically stable, a less stable phase will be formed' [150]. Note that Ostwald restricted his formulation to the possible result of the transformation not specifying the bulk state of the critical clusters as done in the generalization of this rule as given above (see Section 5.4). Implicitly it is assumed in his formulation – and also in its theoretical foundation as developed first by Stranski and Totomanov [151] – that the critical clusters have properties equivalent to the properties of one of the finite number of phases which can exist in a macroscopic form, at least, in a metastable state at the given conditions.

Ostwald's rule is corroborated by the following thermodynamic considerations. Employing the Skapski–Turnbull equation, Eq. (31), to estimate the crystal/liquid interfacial energy, one can show that the thermodynamic barrier for

nucleation is proportional to the melting enthalpy. Hence, higher nucleation rates of metastable phases than those of the stable phase could be expected due to its lower melting enthalpy and correspondingly lower thermodynamic barrier. But a higher nucleation rate of a metastable phase must be accompanied by a lower growth rate, since the latter is proportional to the thermodynamic driving force. This is especially true if the composition of the metastable phase is similar to that of the parent glass.

Once crystallites of a metastable phase form, they may favor nucleation of crystallites of the stable phase if its formation is followed by transformation into aggregates of the more stable phase as discussed in Ref. [152]. Thus, metastable crystals can, in principle, catalyze in one or the other way nucleation processes of the stable phase. Some authors suggested that such crystallization path occurs in $Li_2O\cdot 2SiO_2$ (LS_2) glass, which has been used for many years as a model system to study homogeneous nucleation (see, e.g., [153,154]). An article by Deubener et al. [141] (discussed in Section 5.6) reawakened the interest in this problem and stimulated an intensive search for metastable phase formation in LS_2-glass [155–157], mainly by transmission electron microscopy (TEM) and X-ray diffraction (XRD) methods. In addition to stable lithium disilicate and metastable metasilicate crystals, other, so far unknown, phases were found. However, the observations of different authors were often in contradiction to each other. But, in general, the probability of observing such new phases in LS_2 glass increases with a decrease in time and temperature of heat treatment [158]. Due to low nucleation rates and correspondingly low crystal number densities, and extremely small areas observed by TEM, the statistics of such measurements are quite poor. Moreover, the electron beam can degrade the crystals under study in a short time. As an example, however, the results of Ref. [159] show that at $T = 454$ °C (close to the nucleation rate maximum), only $Li_2O\cdot 2SiO_2$ (LS_2) and $Li_2O\cdot SiO_2$ (LS) crystals were detected in the early stages of crystallization (less than 1% crystallized fraction), but LS crystals were not detected in the most advanced stages (5–10% crystallized fraction). It should be emphasized that, according to the data collected in a time interval 0–100 h at 454 °C, the LS crystals sizes practically do not change, while the LS_2 crystals significantly grow (see Fig. 26). This result agrees with calculations according to which the thermodynamic driving force for LS crystallization in lithium disilicate glass is lower than for LS_2 crystals [160], because a higher thermodynamic driving force also results in higher growth rates. Since there was no evidence of heterogeneous nucleation of lithium disilicate on lithium metasilicate crystals, it was concluded that LS nucleates concurrently with the stable phase LS_2 and disappears with time. Recall that lithium disilicate has a wide range of solid solutions (s/s) formation [143,144]; hence, one can suppose that the critical nuclei are also s/s. Here it should be noted that the technique employed in Ref. [159] did not allow them to distinguish stoichiometric compounds from solid solutions.

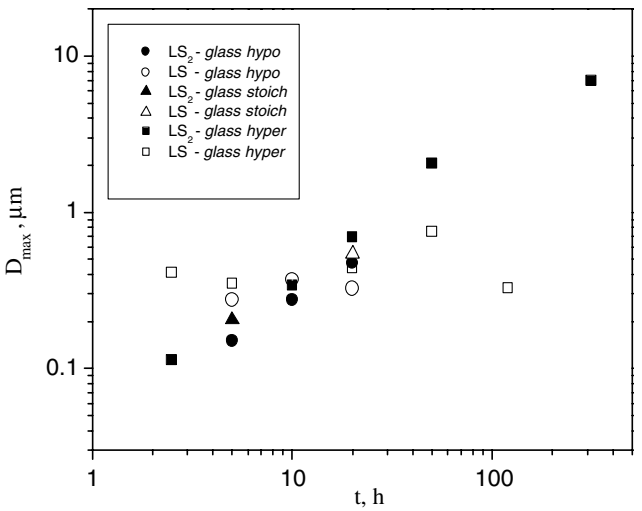

Fig. 26. Maximum dimension (D_{max}) of the largest crystals observed by TEM in samples of *hypo*, *stoich*, and *hyper* lithium disilicate glasses versus heat treatment time at 454 °C [159]. Solid and opened points refer to LS_2 and LS crystals, respectively.

The assumption of s/s nucleation does not contradict the results presented above, but allows one to consider changes of composition of the evolving nuclei with size, such as those demonstrated in Section 5.5 for soda-lime-silica glasses and assumed in Section 5.6. Thus, in some cases, it is possible that the role of metastable phases in nucleation could be simply a continuous variation of nuclei composition (and properties) during the phase transformation. However, there is another factor that has not been taken into consideration so far, but may be of considerable influence. That is the possible effect of elastic stress on nucleation in glass-forming melts. This effect will be analyzed in the next section.

5.8. Effect of elastic stresses on the thermodynamic barrier for nucleation

As it follows from Section 5.1, the thermodynamic barrier for nucleation, W_*, can be calculated in the framework of CNT by a fit of experimental data employing Eq. (34). For such computations, no additional assumptions are needed apart from the validity of CNT. In addition, one has to make some choice concerning the value of the surface energy in the pre-exponential term. However, this choice only weakly affects the final results.

According to Eq. (4), the work of critical cluster formation, W_*, monotonically decreases with decreasing temperature. Nevertheless, the value of $W_*(T/T_m)$, calculated from nucleation data for lithium disilicate glass at temperatures close to T_g shows an anomalous increase with decreasing temperature (cf. Fig. 27). A similar behavior of W_* was observed in other systems, e.g., for wollastonite glass [162]. The above mentioned deviations of the $W_*(T)$-dependence from the expected (according to CNT) may be caused by elastic stresses. Since, in most cases of interest, the crystal densities differ from those of the corresponding

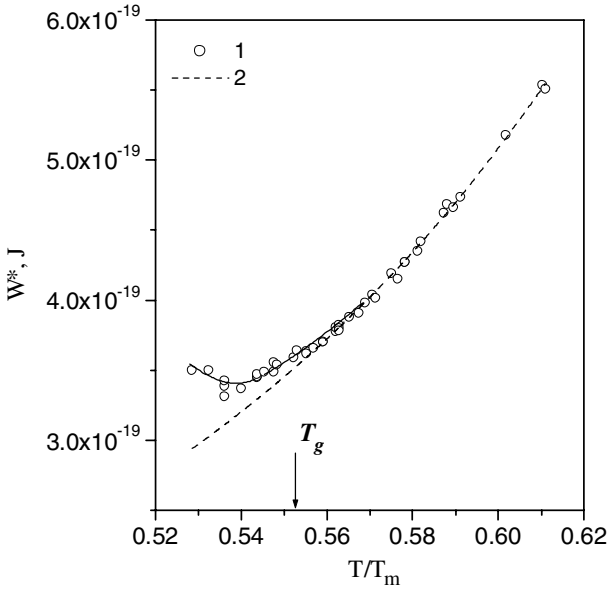

Fig. 27. Thermodynamic barrier for nucleation in $Li_2O \cdot 2SiO_2$-glass (curve 1) estimated from a fit of experimental $I_{st}(T)$ and $t_{ind}(T)$ to Eq. (32), and (curve 2) calculated with Eq. (4) [161].

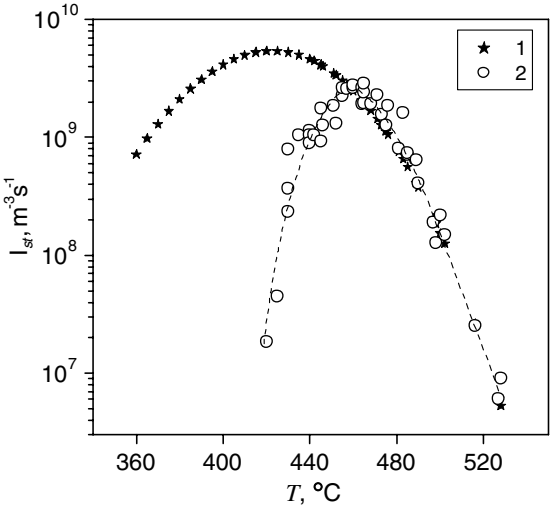

Fig. 28. Temperature dependence of the steady-state nucleation rates in lithium disilicate glass [161]. (points 1) I_{st} calculated with Eq. (34) for the case when elastic stresses do not play any role; (points 2) experimental values of I_{st}. The dashed line is just to guide the eyes.

glasses, glass crystallization is accompanied by volume changes. Such changes may result in stress development which, in turn, diminishes the thermodynamic driving force for the phase transformation by a term connected with the elastic strain energy. This energy can partly or even fully [12,14,163,164] suppress the nucleation-growth process. This effect may be the origin not only of the anomalous behavior of the work of critical cluster formation, $W_*(T)$, but also of a number of well-known additional experimental facts, e.g., the preference of surface to volume nucleation [12,163,164], or the existence of a correlation according to which glasses having densities much lower than those of the corresponding crystals usually reveal only surface crystallization [165].

A theory of nucleation in viscoelastic bodies has been developed recently [166,167] which takes into account both stress development and relaxation in phase formation in glass-forming melts (an analysis of the effect of elastic stresses on crystal growth – based on the same theoretical premises – is given in Ref. [168]). It was concluded that the effect of elastic stresses on nucleation can be remarkable if the time of stress development (estimated as time-lag for nucleation) is smaller than the characteristic time of stress relaxation, which is governed by viscous flow. Such a situation is possible at temperatures lower than the so-called decoupling temperature $T_d \sim 1.2T_g$, when the Stokes–Einstein equation may no longer be valid, i.e., when the nucleation kinetics is *not* governed by viscous flow. A detailed analysis, performed for lithium disilicate glass, shows that elastic stresses may decrease the steady-state nucleation rate by up to two orders of magnitude [169]. In this analysis, the work of critical cluster formation in the absence of elastic stresses was determined following classical nucleation theory.

Recently an attempt was made to estimate the elastic stress energy directly using the deviation of $W_*(T)$-curves from the theoretical one [161] for the same lithium disilicate glass. The obtained values of elastic strain energy were comparable in magnitude with those calculated using the elastic constants of glass and crystals. It should be noted that in the extrapolation of the $W_*(T)$-dependence from relatively high temperatures, at which elastic stress effects can be neglected, to low temperatures, where the minimum of experimental W_*-values is observed, both thermodynamic driving force and crystal/melt surface energy were considered as fit parameters. The fitting procedure produced, in accordance with the conclusions of Section 5.2, values of effective surface energy that decrease with decreasing temperature. Moreover, the thermodynamic driving force turned out to be considerably less than that for the respective macroscopic phase.

Fig. 28 shows experimental steady-state nucleation rates versus temperature together with the theoretical curve calculated by neglecting elastic stresses, employing values for the driving force and surface tension obtained via above discussed fitting procedure. At low temperatures, the calculated I_{st}-values considerably exceed the experimental data giving an indirect evidence of the essential role of elastic stresses in nucleation.

6. Concluding remarks

We presented an overview of experimental results on crystal nucleation in silicate glasses and their theoretical interpretation in the framework of CNT. Different modifications and alternative theoretical approaches of CNT do exist and the importance of the correct determination of the properties of critical clusters and, in particular, of the work for their formation has been known since the

formulation of the basic concepts of CNT. However, following Gibbs' ideas in the description of thermodynamically heterogeneous systems, in the search for the solution of this problem the properties of the critical clusters have been commonly identified with the properties of the newly evolving macroscopic phases. Exclusively under such assumption, the supersaturation (or driving force) can be considered – at constant pressure – as a function only of temperature. As a consequence, in most attempts to reconcile theoretical and experimental results attention was predominantly directed to the determination of the size-dependence of the specific interfacial energy. In contrast, it follows from the present review that the main problem regarding the application of CNT for a quantitative description of nucleation kinetics in glass-forming liquids consists primarily in the adequate description of the bulk properties of the critical nuclei. Of course, a deviation of the bulk properties of the critical clusters as compared with the newly evolving macroscopic phases also leads to modifications of the specific interfacial energy. However, the resulting variation of the specific interfacial energy – due to changes in the bulk properties of the critical clusters as compared with the newly evolving macroscopic phase – is only a secondary factor that must be, of course, also adequately incorporated into the theory. Therefore, the circle of problems one has to solve for the theoretical description of nucleation is enlarged. On the other hand, a new methodology – the generalized Gibbs approach – that allows one to overcome the mentioned problems, which cannot be resolved following the classical concepts of Gibbs, has been recently developed.

Direct experimental methods usually employed to study micron-sized or larger crystals cannot be used for nuclei of critical sizes, which are only of a few nanometers in the temperature range of interest. This is one of the reasons why one typically follows Gibbs' description of heterogeneous systems and assigns the thermodynamic properties (particularly the thermodynamic driving force for crystallization) of the macro-phases to the critical nuclei, thus assuming that the critical nuclei and the evolving stable macro-phase can be characterized by similar bulk state parameters. However, since the thermodynamic barrier for nucleation includes both the thermodynamic driving force and the nucleus-melt surface energy, a maximum thermodynamic driving force (corresponding to the stable phase) is not a necessary condition to attain the lowest value of the thermodynamic barrier and, correspondingly, the highest value of the nucleation rate. Moreover, the thermodynamic properties of the critical nuclei can be affected by elastic stresses arising from differences between the densities of the nucleus and the melt. Hence, one can suppose that, in some cases, the deviation of the composition of the nuclei from those of the stable phase may be accompanied by an approach of the nuclei density to that of the melt. In such cases, the effect of elastic stresses is reduced and, correspondingly, a decrease in the thermodynamic barrier for formation of such nuclei (as compared with the respective value for the stable phase) could be expected. Thus, elastic stress effects can considerably complicate the thermodynamics of nucleation and extend the variety of possible structures and compositions of the critical nuclei.

Since, with rare exceptions, direct measurements of the characteristic properties of critical nuclei are inaccessible, it is rather difficult or impossible to attribute the measured nucleation rates to defined crystal phases. It seems that such situation will not change in the near future. Moreover, taking into account density functional studies, computer simulations and theoretical analyses connected with the generalization of Ostwald's rule of stages, it is even questionable whether the critical clusters have structures and compositions resembling those of the possible macroscopic phases that may evolve in the system under consideration. As shown here, there is some remarkable evidence – partly presented in this review – for the existence of considerable differences between the properties of near-critical nuclei and those of the respective stable macroscopic phases.

Glasses of stoichiometric compositions have been used as model systems in a variety of studies of crystal nucleation. Such choice was made hoping that it should be possible to treat such systems as one-component systems. However, it now became clear that a stoichiometric glass composition, equal to the composition of the evolving crystalline phase, does not guarantee that the nuclei have the same composition. Therefore, systematic investigations of nucleation rates versus glass compositions are of great interest allowing us to understand the true nature of nucleation in glasses. The great value of such analysis is reinforced if the crystal growth rates are also measured in the same temperature range. In this way, additional information can be accumulated allowing one to reveal both the crystal nucleation and growth mechanisms operating in the systems under study.

On the other hand, further development of the classical theories of nucleation and growth – aimed to describe not only critical nuclei formation, but also its subsequent growth, including the possible evolution of their composition – may allow us to develop a more adequate description of phase transformation kinetics. Here we drew attention to a new approach to the description both of nucleation and growth – *the generalized Gibbs' approach* – which has been developed in recent years and already demonstrated its power in the analysis of phase formation in different systems. Existing different alternative theories and modifications of CNT and their further developments will show which of them will be most successful in treating nucleation-growth phenomena in crystallization. However, in order to be successful in the description of experimental data on nucleation and growth, any of the proposed theories – and this is one of the main conclusions of the present review – must be able to appropriately describe the dependence of the properties of the critical clusters on the state of the ambient glass-forming melt and the change of the state of the crystallites with their sizes both in dissolution and

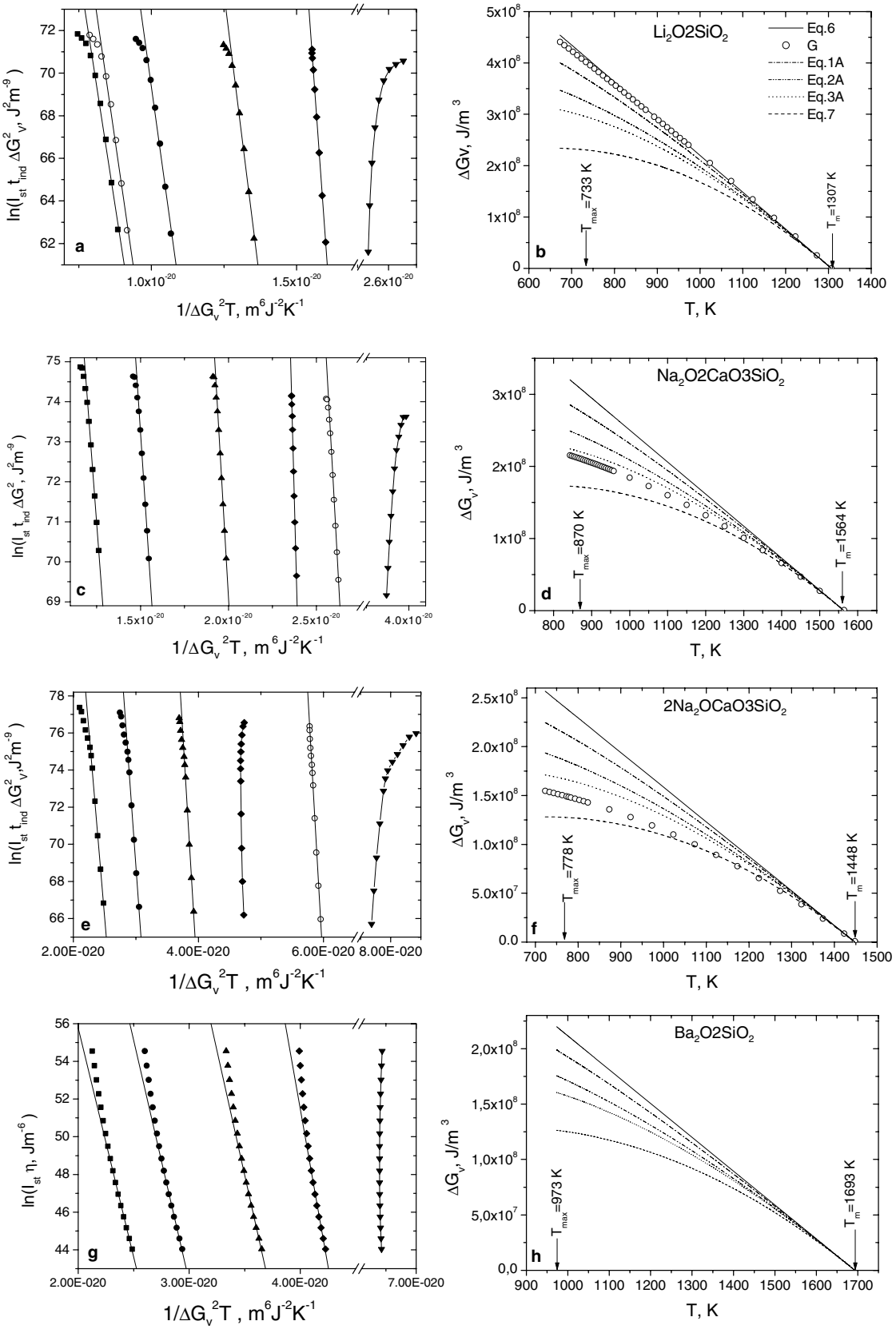

Fig. A1. Analysis of nucleation data with different expressions for the thermodynamic driving force. (b, d, f, h): thermodynamic driving force versus temperature; (a, c, e): $\ln(I_{st}t_{ind}\Delta G_V^2)$; (g): $\ln(I_{st}\eta)$ versus $1/\Delta G_V^2 T$. Opened circles are plotted employing the experimental values of the thermodynamic driving force.

Table A1
Ratio of experimental and theoretical pre-exponential terms, and surface energy for different glasses [40] calculated by fitting nucleation data to CNT employing experimental and approximate values of the thermodynamic driving force

	$Li_2O \cdot 2SiO_2$		$Na_2O \cdot 2CaO \cdot 3SiO_2$		$2Na_2O \cdot CaO \cdot 3SiO_2$		$BaO \cdot 2SiO_2$[a]	
	σ^*_{cm}	$\log\left(\frac{I_o^{exp}}{I_o^{theo}}\right)$	σ^*_{cm}	$\log\left(\frac{I_o^{exp}}{I_o^{theo}}\right)$	σ^*_{cm}	$\log\left(\frac{I_o^{exp}}{I_o^{theo}}\right)$	σ^*_{cm}	$\log\left(\frac{I_o^{exp}}{I_o^{theo}}\right)$
Eq. (6)	0.19	15	0.17	18	0.15	27	0.13	8
Eq. (A.1)	0.20	27	0.18	30	0.16	46	0.13	14
Eq. (A.2)	0.20	45	0.19	51	0.17	79	0.13	23
Eq. (A.3)	0.25	113	0.22	156			0.14	43
Experiment	0.20	19	0.19	72	0.17	139		

The specific interfacial energy is given in $J\,m^{-2}$.
[a] Viscosity was used to calculate I_o^{exp} and σ^*_{cm}.

growth processes. We believe the analysis of the size-dependence of the cluster properties and their theoretical interpretation may lead to new exciting developments in the field of crystal nucleation of glasses, with a variety of new applications. Thus, despite the fact that numerous analyses of crystallization kinetics and mechanisms of silicate and other glasses have been performed for decades, they are expected to remain a highly interesting subject for both fundamental and applied research on nucleation and phase transformations in general.

Acknowledgements

The authors thank Fapesp, Capes and CNPq (Brazil) for their financial support of this work.

Appendix A

The experimental values of the thermodynamic driving force for crystallization given by Eq. (5) is bounded by a linear approximation (Eq. (6)), commonly denoted as Turnbull's formula, and by the approximation of Hoffman (Eq. (7)), see Fig. A1(b), (d), and (f). Eq. (6) directly follows from Eq. (5) in the case of $\Delta C_p = 0$. The Hoffman equation assumes $\Delta C_p =$ constant and some additional simplifications. There are other approximations that predict values of ΔG_V located inside the range given by Eqs. (6) and (7). Some of them, taken from Ref. [13], are

$$\Delta G_V = \frac{\Delta H_V \Delta T}{T_m}\left[\frac{7T}{T_m + 6T}\right], \tag{A.1}$$

$$\Delta G_V = \frac{\Delta H_V \Delta T}{T_m} - \gamma \Delta S_m\left[\Delta T - T\ln\left(\frac{T_m}{T}\right)\right], \tag{A.2}$$

$$\Delta G_V = \frac{\Delta H_V \Delta T}{T_m}\frac{2T}{T_m + T}. \tag{A.3}$$

Fig. A1(b), (d), (f), and (h) shows the values of ΔG_V versus temperature calculated with Eqs. (6), (A.1), (A.2), (A.3), and (7). The value of γ in Eq. (A.2) was chosen equal to 0.8. Experimental data on ΔG_V are also shown for $Li_2O \cdot 2SiO_2$, $Na_2O \cdot 2CaO \cdot 3SiO_2$ and $2Na_2O \cdot 1CaO \cdot 3SiO_2$ glasses. Different approximations for the thermodynamic driving force were used to plot the nucleation rates as shown in Fig. A1(a), (c), (e), and (g). The intercepts and slopes of the linear fits at $T > T_g$ were employed to estimate I_o^{exp} and σ^*_{cm}. These parameters are listed in Table A1.

According to Table A1 the discrepancy between experimental and theoretical values of I_o is always drastic and becomes even stronger when the $\Delta G_V(T)$-function becomes weaker, while σ^*_{cm} depends only weakly on the choice of a particular expression for the thermodynamic driving force.

References

[1] J.W.P. Schmelzer, in: J.W.P. Schmelzer, G. Röpke, V.B. Priezzhev (Eds.), Nucleation Theory and Applications, Joint Institute for Nuclear Research Publishing Department, Dubna, Russia, 1999, p. 1.
[2] J.M.F. Navaro, El Vidrio, CSIC, Madrid, Spain, 1991.
[3] W. Höland, G. Beall, Glass-ceramic technology, American Ceramic Society, 2002.
[4] J.W. Gibbs, The Collected Works, Thermodynamics, vol. 1, Longmans & Green, New York, 1928.
[5] R. Kaischew, I.N. Stranski, Z. Phys. Chem. B 26 (1934) 317.
[6] M. Volmer, A. Weber, Z. Phys. Chem. 119 (1926) 277.
[7] R. Becker, W. Döring, Ann. Phys. 24 (1935) 719;
R. Becker, Ann. Phys. 32 (1938) 128.
[8] M. Volmer, Kinetik der Phasenbildung, Steinkopf, Dresden, 1939.
[9] J. Frenkel, Kinetic Theory of Liquids, Oxford University Press, Oxford, 1946.
[10] D. Turnbull, J.C. Fisher, J. Chem. Phys. 17 (1949) 71.
[11] H. Reiss, J. Chem. Phys. 18 (1950) 840.
[12] I. Gutzow, J. Schmelzer, The Vitreous State: Thermodynamics, Structure, Rheology and Crystallization, Springer, Berlin, 1995.
[13] K.F. Kelton, Solid State Phys. 45 (1991) 75.
[14] J.W. Christian, The Theory of Transformations in Metals and Alloys. Part I, Pergamon Press, Oxford, 1981.
[15] F.C. Collins, Z. Electrochem. 59 (1955) 404.
[16] D. Kashchiev, Surf. Sci. 14 (1969) 209.
[17] V.N. Filipovich, V.M. Fokin, N.S. Yuritsyn, A.M. Kalinina, Thermochim. Acta 280&281 (1996) 205.
[18] G. Tammann, Z. Phys. Chem. 25 (1898) 441.
[19] M. Ito, T. Sakaino, T. Moriya, Bull. Tokyo Inst. Technol. 88 (1968) 127.
[20] V.N. Filipovich, A.M. Kalinina, Izv. Akad. Nauk USSR, Neorgan. Mat. 4 (1968) 1532 (in Russian).
[21] I. Gutzow, Contemp. Phys. 21 (1980) 121, 243.
[22] S. Toschev, I. Gutzow, Phys. Status Solidi 24 (1967) 349.
[23] U. Köster, Mater. Sci. Eng. 97 (1988) 183.
[24] V.M. Fokin, N.S. Yuritsyn, V.N. Filipovich, A.M. Kalinina, J. Non-Cryst. Solids 219 (1997) 37.
[25] E.D. Zanotto, P.F. James, J. Non-Cryst. Solids 124 (1990) 86.

[26] E.D. Zanotto, J. Mater. Res. 13 (1998) 2045.
[27] S. Toschev, in: P. Hartman (Ed.), Crystal Growth: An Introduction, North-Holland Publishing Company, Amsterdam, 1973, p. 1.
[28] V.P. Skripov, V.P. Koverda, Spontaneous Crystallization of Supercooled Liquids, Nauka, Moscow, 1984 (in Russian).
[29] A.N. Kolmogorov, Izv. Akad. Nauk USSR, Ser. Mathem. 3 (1937) 355 (in Russian).
[30] W.A. Johnson, R.F. Mehl, Trans. AIME 135 (1939) 416.
[31] M. Avrami, J. Chem. Phys. 7 (1939) 1103.
[32] V.N. Filipovich, A.M. Kalinina, V.M. Fokin, E.K. Shischkina, D.D. Dmitriev, Fiz. Khim. Stekla 9 (1983) 58 [English trans.: Soviet J. Glass Phys. Chem. 9 (1983) 45].
[33] E.D. Zanotto, A.C. Galhardi, J. Non-Cryst. Solids 103 (1982) 73.
[34] A.A. Cabral, V.M. Fokin, E.D. Zanotto, J. Non-Cryst. Solids 330 (2003) 174.
[35] V.M. Fokin, A.M. Kalinina, V.N. Filipovich, J. Cryst. Growth 52 (1980) 115.
[36] A.M. Kalinina, V.M. Fokin, V.N. Filipovich, J. Non-Cryst. Solids 38&39 (1980) 723.
[37] U. Schiffner, W. Pannhorst, Glastech. Ber. 60 (1987) 211.
[38] A.M. Kalinina, V.M. Fokin, V.N. Filipovich, Fiz. Khim. Stekla 2 (1976) 298 [English trans.: Soviet J. Glass Phys. Chem. 2 (1976) 294].
[39] I. Gutzow, S. Toschev, M. Marinov, E. Popov, Kristall Technik 3 (1968) 337.
[40] E.D. Zanotto, V.M. Fokin, Phil. Trans. R Soc. Lond. A 361 (2002) 591.
[41] V.M. Fokin, A.M. Kalinina, V.N. Filipovich, Fiz. Khim. Stekla 3 (1977) 122 [English trans.: Soviet J. Glass Phys. Chem. 3 (1977) 113].
[42] S.C. Glotzer, J. Non-Cryst. Solids 274 (2000) 342.
[43] V.M. Fokin, A.M. Kalinina, V.N. Filipovich, Fiz. Khim. Stekla 3 (1977) 129 [English trans.: Soviet J. Glass Phys. Chem. 3 (1977) 119].
[44] Z. Kozisek, Cryst. Res. Technol. 23 (1988) 1315.
[45] K.F. Kelton, A.L. Greer, Phys. Rev. B 38 (1988) 10089.
[46] A.L. Greer, K.F. Kelton, J. Am. Ceram. Soc. 74 (1991) 1015.
[47] J. Deubener, in: Proc. XIX Int. Cong. on Glass, vol. 2, Extended Abstracts, Soc. Glass Technology, Edinburgh, 2001, p. 66.
[48] O.V. Potapov, V.M. Fokin, V.L. Ugolkov, L.Y. Suslova, V.N. Filipovich, Glass Phys. Chem. 26 (2000) 39.
[49] D. Turnbull, J. Chem. Phys. 18 (1950) 769.
[50] A.S. Skapski, Acta Metall. 4 (1956) 576.
[51] A.M. Kalinina, V.N. Filipovich, V.M. Fokin, G.A. Sycheva, in: Proc. XIV Int. Cong. on Glass, vol. 1, New Delhi, 1986, p. 366.
[52] O.V. Potapov, V.M. Fokin, V.N. Filipovich, J. Non-Cryst. Solids 247 (1999) 74.
[53] R. Müller, E.D. Zanotto, V.M. Fokin, J. Non-Cryst. Solids 274 (2000) 208.
[54] G. Tammann, Z. Elektrochemie 10 (1904) 532.
[55] P.F. James, in: M.H. Lewis (Ed.), Glasses and Glass-Ceramics, Chapman and Hall, London, 1989, p. 59.
[56] E.D. Zanotto, J. Non-Cryst. Solids 89 (1987) 361.
[57] J. Deubener, J. Non-Cryst. Solids 274 (2000) 195.
[58] V.M. Fokin, E.D. Zanotto, J.W.P. Schmelzer, J. Non-Cryst. Solids 321 (2003) 52.
[59] M.H. Lewis, J. Metacalf-Johanson, P.S. Bell, J. Am. Ceram. Soc. 62 (1979) 278.
[60] D. Turnbull, in: J.A. Prins (Ed.), Physics of Non-Crystalline Solids, North Holland Publishing Company, Amsterdam, 1965, p. 41.
[61] G. Tammann, Der Glaszustand, Leopold Voss Verlag, Leipzig, 1933.
[62] G.L. Mikhnevich, J.F. Browko, Phys. Sowjetunion 13 (1938) 113.
[63] P.F. James, in: J.H. Simmons, D.R. Uhlmann, G.H. Beall (Eds.), Advances in Ceramics, vol. 4, American Ceramic Society, Columbus, Ohio, 1982, p. 1.
[64] M.C. Weinberg, E.D. Zanotto, J. Non-Cryst. Solids 108 (1989) 99.
[65] Y. Miyazawa, G.M. Pound, J. Cryst. Growth 23 (1974) 45.
[66] D. Turnbull, J. Chem. Phys. 20 (1952) 411.
[67] L. Shartsis, S. Spinner, J. Res. Nat. Bur. Stand. 46 (1951) 385.
[68] A.A. Appen, K.A. Schishov, S.S. Kaylova, Silikattechnik 4 (1953) 104.
[69] V.M. Fokin, E.D. Zanotto, J.W.P. Schmelzer, J. Non-Cryst. Solids 278 (2000) 24.
[70] J. Stefan, Ann. Phys. 29 (1886) 655.
[71] V.M. Fokin, E.D. Zanotto, J. Non-Cryst. Solids 265 (2000) 105.
[72] I. Gutzow, D. Kashchiev, I. Avramov, J. Non-Cryst. Solids 73 (1985) 477.
[73] A.I. Rusanov, Phasengleichgewichte und Grenzflächenerscheinungen, Akademie-Verlag, Berlin, 1978.
[74] V.P. Skripov, M.Z. Faizulin, in: J.W.P. Schmelzer (Ed.), Nucleation Theory and Applications, Wiley-VCH, Berlin-Weinheim, 2005, p. 4.
[75] F. Spaepen, Solid State Phys. 47 (1994) 1.
[76] V.N. Filipovich, T.A. Zhukovskaya, Fiz. Khim. Stekla 14 (1988) 300 (in Russian).
[77] L. Granasy, P. James, J. Non-Cryst. Solids 253 (1999) 210.
[78] L. Granasy, T. Börzsony, T. Pusztai, J. Cryst. Growth 237 (2002) 1813.
[79] J.W.P. Schmelzer, G.Sh. Boltachev, V.G. Baidakov, in: J.W.P. Schmelzer (Ed.), Nucleation Theory and Applications, Wiley-VCH, Berlin-Weinheim, 2005, p. 418.
[80] V.G. Baidakov, G.Sh. Boltachev, J.W.P. Schmelzer, J. Colloid Interface Sci. 231 (2000) 312.
[81] V.G. Baidakov, J.W.P. Schmelzer, J. Phys. Chem. B 105 (2001) 11595.
[82] J.W. P Schmelzer, V.G. Baidakov, G.Sh. Boltachev, J. Chem. Phys. 119 (2003) 6166.
[83] J.D. van der Waals, Ph. Kohnstamm, Lehrbuch der Thermodynamik, Johann-Ambrosius-Barth Verlag, Leipzig und Amsterdam, 1908.
[84] J.D. van der Waals, Z. Phys. Chem. 13 (1893) 657 (in German) [J.S. Rowlinson, Translation of J.D. van der Waals': The thermodynamic theory of capillarity under the hypothesis of a continuous variation of density, J. Stat. Phys. 20 (1979) 197].
[85] J.W. Cahn, J.E. Hilliard, J. Chem. Phys. 28 (1959) 258;
J.W. Cahn, J.E. Hilliard, J. Chem. Phys. 31 (1959) 688.
[86] D.W. Oxtoby, R. Evans, J. Chem. Phys. 89 (1988) 7521.
[87] C.K. Bagdassarian, D.W. Oxtoby, J. Chem. Phys. 100 (1994) 2139.
[88] D.W. Oxtoby, Acc. Chem. Res. 31 (1998) 91.
[89] L. Granasy, J. Mol. Struct. 485&486 (1999) 523.
[90] L. Granasy, T. Pusztai, P. James, J. Chem. Phys. 117 (2002) 6157.
[91] J.W.P. Schmelzer, A.S. Abyzov, J. Möller, J. Chem. Phys. 121 (2004) 6900.
[92] B.N. Hale, in: M. Kasahara, M. Kulmala (Eds.), 16th Int. Conf. on Nucleation and Atmospheric Aerosols, Kyoto, Japan, August 2004, compact disk.
[93] P.R. ten Wolde, D. Frenkel, J. Chem. Phys. 109 (1998) 9919.
[94] V.K. Shen, P.G. Debenedetti, J. Chem. Phys. 111 (1999) 3581.
[95] K. Laasonen, S. Wonczak, R. Strey, A. Laaksonen, J. Chem. Phys. 113 (2000) 9741.
[96] B. Chen, J.I. Siepmann, K.J. Oh, M.L. Klein, J. Chem. Phys. 115 (2000) 10903.
[97] J.W.P. Schmelzer, J. Schmelzer Jr., I. Gutzow, J. Chem. Phys. 112 (2000) 3820.
[98] J.W.P. Schmelzer, in: J.W.P. Schmelzer (Ed.), Nucleation Theory and Applications, Wiley-VCH, Berlin-Weinheim, 2005, p. 447.
[99] H. Ulbricht, J.W.P. Schmelzer, R. Mahnke, F. Schweitzer, Thermodynamics of Finite Systems and the Kinetics of First-Order Phase Transitions, Teubner, Leipzig, 1988.
[100] J.W.P. Schmelzer, V.G. Baidakov, J. Chem. Phys., submitted for publication.
[101] J.W.P. Schmelzer, Phys. Chem. Glasses 45 (2004) 116.
[102] J.W.P. Schmelzer, A.R. Gokhman, V.M. Fokin, J. Colloid Interface Sci. 272 (2004) 109.
[103] J.W.P. Schmelzer, in: XX Int. Cong. on Glass, Kyoto, 2004, compact disk.

[104] J.W.P. Schmelzer, A.S. Abyzov, in: J.W.P. Schmelzer, G. Röpke, V.B. Priezzhev (Eds.), Nucleation Theory and Applications, Joint Institute for Nuclear Research Publishing Department, Dubna, Russia, 2006, p. 4.
[105] L. Granasy, P.F. James, J. Chem. Phys. 113 (2000) 9810.
[106] D. Tatchev, G. Goerigk, E. Valova, J. Dille, R. Kranold, S. Armyanov, J.-L. Delplancke, Appl. Crystallogr. 38 (2005) 787.
[107] D. Tatchev, A. Hoell, R. Kranold, S. Armyanov, Physica B 369 (2005) 8.
[108] P.J. Desre, E. Cini, B. Vinet, J. Non-Cryst. Solids 288 (2001) 210.
[109] W. Pan, A.B. Kolomeisky, P.G. Vekilov, J. Chem. Phys. 122 (2005) 174905.
[110] G. Medeiros-Ribeiro, A.M. Bratkovski, T.I. Kamins, D.A.A. Ohlberg, R.S. Williams, Science 286 (1998) 353.
[111] F.M. Ross, R.M. Tromp, M.C. Reuter, Science 286 (1999) 1931.
[112] A. Rastelli, M. Kummer, H. van Käse, Phys. Rev. Lett. 87 (2001) 256101.
[113] P.G. Debenedetti, H. Reiss, J. Chem. Phys. 108 (1998) 5498, and references cited therein.
[114] D.W. Oxtoby, Nature 347 (1990) 725.
[115] L. Granasy, T. Börzsony, T. Pusztai, Phys. Rev. Lett. 20 (2002) 206105.
[116] L. Granasy, T. Pusztai, J.A. Warren, J. Phys.: Cond. Matter. 16 (2004) R1205.
[117] T. Pusztai, G. Bortel, L. Granasy, Europhys. Lett. 71 (2005) 131.
[118] T. Pusztai, G. Bortel, L. Granasy, Mater. Sci. Eng. A 413&414 (2005) 412.
[119] V.P. Skripov, V.G. Baidakov, High Temp. Thermal Phys. 10 (1972) 1226 (in Russian).
[120] L.D. Landau, I.M. Lifschitz, Statistische Physik, Akademie-Verlag, Berlin, 1976.
[121] V.P. Skripov, M.Z. Faizullin, Solid–Liquid–Gas Phase Transitions and Thermodynamic Similarity, Wiley-VCH, Berlin-Weinheim, 2006.
[122] L. Granasy, T. Wang, P. James, J. Chem. Phys. 108 (1998) 7317.
[123] L. Granasy, D.W. Oxtoby, J. Chem. Phys. 112 (2000) 2410.
[124] L. Granasy, T. Pusztai, J. Chem. Phys. 117 (2002) 10121.
[125] D. Kashchiev, J. Chem. Phys. 76 (1984) 5098.
[126] D.W. Oxtoby, D. Kashchiev, J. Chem. Phys. 100 (1994) 7665.
[127] J.W.P. Schmelzer, J. Colloid Interface Sci. 242 (2001) 354.
[128] J.W.P. Schmelzer, Russ. J. Phys. Chem. 77 (2003) 143.
[129] Y. Viisanen, R. Strey, H. Reiss, J. Chem. Phys. 99 (1993) 4680.
[130] Y. Viisanen, R. Strey, J. Chem. Phys. 105 (1996) 8293.
[131] V.G. Karpov, D.W. Oxtoby, Phys. Rev. 54 (1996) 9734.
[132] M.F. Thorpe, J. Non-Cryst. Solids 57 (1983) 355.
[133] M.F. Thorpe, M.I. Mitkova (Eds.), Amorphous insulators and semiconductors, NATO ASI, Kluwer, Dordrecht, 1997.
[134] I. Avramov, R. Keding, C. Rüssel, R. Kranold, J. Non-Cryst. Solids 278 (2001) 13.
[135] B.A. Shakhmatkin, N.M. Vedishcheva, J. Non-Cryst. Solids 171 (1994) 1.
[136] B.A. Shakhmatkin, N.M. Vedishcheva, M.M. Shultz, A.C. Wright, J. Non-Cryst. Solids 177 (1994) 249.
[137] V.M. Fokin, O.V. Potapov, E.D. Zanotto, F.M. Spiandorello, V.L. Ugolkov, B.Z. Pevzner, J. Non-Cryst. Solids 331 (2003) 240.
[138] E.N. Soboleva, N.S. Yuritsyn, V.L. Ugolkov, Glass Phys. Chem. 30 (2004) 481.
[139] G. Völksch, T. Kittel, F. Siegelin, H.-J. Kleebe, in: XIX Int. Cong. on Glass, Edinburgh, 2001.
[140] M. Roskosz, M.J. Toplis, P. Besson, P. Richet, J. Non-Cryst. Solids 351 (2005) 1266.
[141] J. Deubener, R. Brückner, M. Sternitzke, J. Non-Cryst. Solids 163 (1993) 1.
[142] N.S. Yuritsyn, J.W.P. Schmelzer, V.M. Fokin, E.D. Zanotto, In preparation.
[143] A.R. West, F.P. Glasser, in: L.L. Hench, S.W. Freiman (Eds.), Advances in Nucleation and Crystallization in Glasses, American Ceramic Society, Columbus, Ohio, 1971, p. 151.
[144] I. Hasdemir, R. Brückner, J. Deubener, Phys. Chem. Glasses 39 (1998) 253.
[145] E.D. Zanotto, M.L.G. Leite, J. Non-Cryst. Solids 202 (1996) 145.
[146] M.C. Weinberg, J. Non-Cryst. Solids 170 (1994) 300.
[147] V.V. Slezov, J.W.P. Schmelzer, in: J.W.P. Schmelzer, G. Röpke, V.B. Priezzhev (Eds.), Nucleation Theory and Applications, Joint Institute for Nuclear Research Publishing Department, Dubna, Russia, 1999, p. 6.
[148] K.S. Russell, Acta Metall. 16 (1968) 761.
[149] K.F. Kelton, Acta Mater. 48 (2000) 1967.
[150] W. Ostwald, Z. Phys. Chem. 22 (1897) 289.
[151] I. Stranski, D. Totomanov, Z. Phys. Chem. A 163 (1933) 399.
[152] A.S. Milev, I.S. Gutzow, Bulg. Chem. Commun. 29 (1996/1997) 597.
[153] A.M. Kalinina, V.N. Filipovich, V.A. Kolesova, I.A. Bondar, in: E.A. Porai-Koshits (Ed.), The Structure of Glass, vol. 3, Consultants Bureau, New York, 1964, p. 53.
[154] D.L. Kinser, L.L. Hench, J. Am. Ceram. Soc. 12 (1971) 58.
[155] P.C. Soares Jr., Initial stages of crystallization in lithium disilicate glass revisited, MSc thesis, Universidade Federal de São Carlos, Brazil, 1997 (in Portuguese).
[156] Y. Iqbal, W.E. Lee, D. Holland, P.F. James, J. Non-Cryst. Solids 224 (1998) 1.
[157] L.I. Burger, P. Lucas, M.C. Weinberg, P.C. Soares Jr., E.D. Zanotto, J. Non-Cryst. Solids 274 (2000) 188.
[158] J. Deubener, Homogene Volumenkeimbildung in Silicatschmelzen: Theorie und Experiment, Habilitationsschrift, Berlin, 2001.
[159] P.C. Soares Jr., E.D. Zanotto, V.M. Fokin, H.J. Jain, J. Non-Cryst. Solids 331 (2003) 217.
[160] B.A. Shakhmatkin, N.M. Vedishcheva, Private communication, 2001.
[161] V.M. Fokin, E.D. Zanotto, J.W.P. Schmelzer, O.V. Potapov, J. Non-Cryst. Solids 351 (2005) 1491.
[162] L. Granasy, T. Pusztai, P.F. James, J. Chem. Phys. 117 (2002) 6157.
[163] J.W.P. Schmelzer, R. Pascova, J. Möller, I. Gutzow, J. Non-Cryst. Solids 162 (1993) 26.
[164] J.W.P. Schmelzer, J. Möller, I. Gutzow, R. Pascova, R. Müller, W. Pannhorst, J. Non-Cryst. Solids 183 (1995) 215.
[165] E.D. Zanotto, E.J. Müller, J. Non-Cryst. Solids 130 (1991) 220.
[166] J.W.P. Schmelzer, R. Müller, J. Möller, I.S. Gutzow, Phys. Chem. Glasses 43C (2002) 291.
[167] J.W.P. Schmelzer, R. Müller, J. Möller, I.S. Gutzow, J. Non-Cryst. Solids 315 (2003) 144.
[168] J.W.P. Schmelzer, E.D. Zanotto, I. Avramov, V.M. Fokin, J. Non-Cryst. Solids 352 (2006) 434.
[169] J.W.P. Schmelzer, O.V. Potapov, V.M. Fokin, R. Müller, S. Reinsch, J. Non-Cryst. Solids 333 (2004) 150.